Burst mitofusin activation reverses neuromuscular dysfunction in murine CMT2A

Antonietta Franco[1#], Xiawei Dang[1,2#], Emily K. Walton[1], Joshua N. Ho[3,4], Barbara Zablocka[5], Cindy Ly[6], Timothy M. Miller[6], Robert H. Baloh[7], Michael E. Shy[8], Andrew S. Yoo[3,4], Gerald W. Dorn II[1].

[1]Department of Internal Medicine, Washington University School of Medicine, St. Louis MO USA.

[2]Department of Cardiology, The First Affiliated Hospital of Xi'an Jiao Tong University, Xi'an, Shaanxi, China.

[3]Department of Developmental Biology, Washington University School of Medicine, St. Louis, MO, USA

[4]Center for Regenerative Medicine, Washington University School of Medicine, St. Louis, MO, USA

[5]Mossakowski Medical Research Centre, Polish Academy of Sciences, Warsaw, Poland

[6]Department of Neurology, Washington University School of Medicine, St. Louis, MO, USA

[7]Department of Neurology, Cedars-Sinai Medical Center, Los Angeles, CA USA.

[8]Department of Neurology, Carver College of Medicine, University of Iowa, Iowa City, IA, USA

# Contributed equally

Correspondence to:
Gerald W. Dorn II, MD
Philip and Sima K. Needleman Professor
Washington University Center for Pharmacogenomics
660 S Euclid Ave.
Campus Box 8220 St. Louis, MO 63110
Phone: 314 362-4892. Fax 314 362-8844.
Email: gdorn@wustl.edu

Abstract

Charcot-Marie-Tooth disease type 2A (CMT2A) is an untreatable childhood peripheral neuropathy caused by mutations of the mitochondrial fusion protein, mitofusin (MFN) 2. Here, pharmacological activation of endogenous normal mitofusins overcame dominant inhibitory effects of CMT2A mutants in reprogrammed human patient motor neurons, reversing hallmark mitochondrial stasis and fragmentation independent of causal *MFN2* mutation. In mice expressing human *MFN2* T105M, intermittent mitofusin activation with a small molecule, MiM111, normalized CMT2A neuromuscular dysfunction, reversed pre-treatment axon and skeletal myocyte atrophy, and enhanced axon regrowth by increasing mitochondrial transport within peripheral axons and promoting *in vivo* mitochondrial localization to neuromuscular junctional synapses. MiM111-treated *MFN2* T105M mouse neurons exhibited accelerated primary outgrowth and greater post-axotomy regrowth, linked to enhanced mitochondrial motility. MiM111 is the first pre-clinical candidate for CMT2A.

Introduction

Charcot-Marie-Tooth disease (CMT) describes a family of genetically diverse and clinically heterogeneous peripheral neuropathies [1]. Type 2A CMT (CMT2A) is caused by mutations of the mitochondrial fusion protein, mitofusin 2 (*MFN2*) [2], and is distinguished from other CMT subtypes by onset of neuromuscular signs in early childhood and progressive loss of neuromuscular coordination and strength in arms throughout the first two decades of life, thought to be the consequence of dying-back of long peripheral nerves [1,3-6]. Because there are currently no disease-modifying treatments, CMT2A is managed with braces, wheelchairs, and social support.

Over 100 different dominant missense *MFN2* mutations are implicated in CMT2A[7]. MFN2 and related MFN1 are nuclear-encoded dynamin-family GTPases located at the mitochondrial outer membrane-cytosol interface where they promote mitochondrial fusion essential to mitochondrial respiratory function and repair [8]. Dominant inhibition by MFN2 mutants of mitochondrial fusion [9,10], mitophagy [11,12], and/or neuronal mitochondrial transport [10,13,14] are proposed to evoke neuronal degeneration in CMT2A.

Because CMT2A is an autosomal dominant genetic condition, gene editing could potentially correct causal *MFN2* mutant alleles, but the large number of different causal CMT2A *MFN2* mutations complicates an editing approach. Alternately, forced expression of normal mitofusins could oppose mutant *MFN2* dysfunction, as demonstrated in a recent study in transgenic mice [15]. However, MFN gene therapy would be difficult to discontinue or reverse if postulated adverse effects of MFN overactivity are encountered[16]. Here, we describe a therapeutic approach to CMT2A that is agnostic to *MFN2* genotype and does not require genetic manipulation: intermittent or "burst" activation of endogenous normal mitofusins. Pharmacological mitofusin activators improved mitochondrial morphology, fitness, and motility in human and mouse CMT2A neurons *in vitro*. Daily administration of a short acting mitofusin activator to mice with late stage CMT2A reversed neuromuscular dysfunction. Mechanistically, neuronal repair and regeneration were linked to enhanced mitochondrial transport to, and mitochondrial occupation within, axonal termini. Reversal of pre-existing CMT2A neuromuscular degeneration *in vivo* has not previously been achieved by any means, and provides a powerful rationale for advancing mitofusin activators to first in human trials.

Results:

Genetically diverse CMT2A patient neurons exhibit similar mitochondrial phenotypes

One of the central features of CMT2A is the large number of different *MFN2* mutations that provoke the syndrome. Common MFN2 GTPase and coiled-coiled domain mutations induce more severe and earlier onset disease, whereas rare carboxy terminal domain mutations confer later onset and milder disease [3,17]. We compared mitochondrial phenotypes in cells from four CMT2A patients, two having *MFN2* mutations within the canonical Dynamin/Fzo-like GTPase domain (*MFN2* T105M in the G1 motif and *MFN2* R274W between the G4 and G5 motifs), and two with mutations in the *MFN2* coiled-coiled helix bundle core (*MFN2* H361Y and R364W). **(Figure 1**- figure supplement 1). Donor patient characteristics are in **Table 1.**

To avoid loss of some CMT2A-associated mitochondrial phenotypes in iPSC-derived neurons [11,18], we directly reprogrammed CMT2A patient fibroblasts into motor neurons via microRNA-mediated neuronal conversion (**Figure 1b**) [19]. Reprogramming efficiency was

Diseases	Mutation	Age	Sex	Passage#	Source	Fibroblast ID
CMT2A	*MFN2* Thr105Met	41	F	P4-P10	Dr. Robert H. Baloh	-
CMT2A	*MFN2* Arg274Trp	23	M	P4-P10	Dr. Barbara Zablocka	-
CMT2A	*MFN2* His361Tyr	41	M	P4-P10	Dr. Robert H. Baloh	-
CMT2A	*MFN2* His364Trp	28	F	P6-P10	Dr. Michael E. Shy	-
CMT1A	*PMP22* DUP	28	F	P4-P10	Coriell Institute	GM05167
CTRL 1	-	68	F	P3-P7	NINDS	ND34769
CTRL 2	-	71	F	P3-P7	NINDS	ND36320
CTRL 3	-	55	F	P3-P7	NINDS	ND29510
CTRL 4	-	66	M	P8-P10	NINDS	ND29178
CTRL 5	-	72	M	P3-P7	NINDS	ND34770
CTRL 6	-	55	M	P4-P10	NINDS	ND38530

Table 1. Characteristics and sources of human primary fibroblasts used for motor neuron reprogramming studies

similar between CMT2A and control patient fibroblasts: >90% neurons (measured as β-III tubulin staining), and >85% motor neurons (measured as β-III tubulin, HB9/MNX1 co-staining) (Figure 1 -figure supplement 2). Compared to neurons reprogrammed from individuals with no evident disease at the time of sampling and who had none of the tested MFN2 mutations by Sanger sequencing ("normal"), all four CMT2A motor neuron lines exhibited fragmented mitochondria (decreased mitochondrial aspect ratio; length/width) that is a consequence of impaired fusion in this context [20]; accompanying mitochondrial depolarization reflected characteristic functional impairment (**Figure 1c**) [21]. Moreover, all four CMT2A motor neuron lines exhibited abnormal mitochondrial transport through axons, with diminished proportion and velocity of motile mitochondria (**Figure 1c**). Mitochondrial fragmentation, respiratory dysfunction, and dysmotility observed in reprogrammed neurons are prototypical features of CMT2A [13,15,22,23].

Dominant inhibition of normal *MFN*1 and *MFN2* by CMT2A *MFN2* mutants produces an imbalance between mitochondrial fission and fusion that underlies mitochondrial pathology in CMT2A [15]. This dynamic imbalance can be reversed in transfected mouse cells and *in vivo* mouse models by forced overexpression of normal MFN1 or MFN2 [15,24]. We posited that pharmacological activation of normal endogenous human *MFN1* and *MFN2*

would also reverse mitochondrial abnormalities in CMT2A patient motor neurons. Chimera C is one of a new class of direct mitofusin activators that promotes conformational activation of MFN1 and MFN2, thereby stimulating endogenous mitofusins to improve mitochondrial dysmorphology and dysfunction [23,25]. Chimera C (100 nM, 48h) enhanced mitochondrial fusion (i.e. it increased aspect ratio) and improved respiratory function (i.e. it reversed mitochondrial depolarization) in cells lacking either MFN1 or MFN2, but had no effects in cells lacking both mitofusin targets (Figure 1 -figure supplement 3). Chimera C (100 nM, 48h) also improved mitochondrial aspect ratio, depolarization, and motility in all four CMT2A patient motor neuron lines (**Figure 1c**).

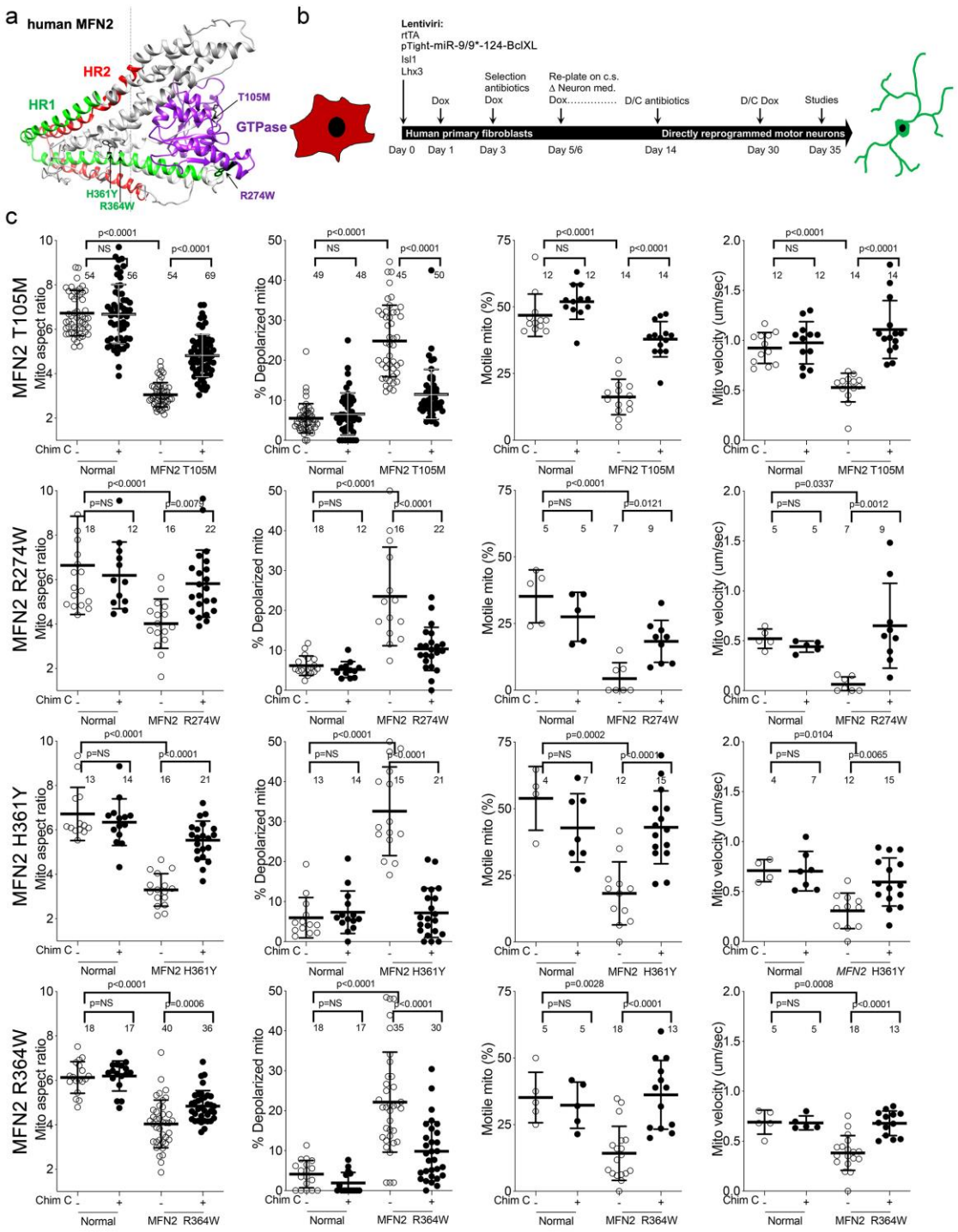

Figure 1. *Mitochondrial abnormalities in reprogrammed CMT2A patient motor neurons and their improvement after mitofusin activation.* **a.** Model structure of *MFN2* showing location of CMT2A patient mutations. **b.** Schematic depiction of fibroblast reprogramming procedure to produce motor neurons. **c.** Mitochondrial testing in reprogrammed motor neurons from four CMT2A patients with different MFN2 mutations and representative of three normal control subjects. Open circles are baseline; closed circles are 48 hours after addition of mitofusin activator Chimera C (100 nM). Each circle is one neuron from 2 or 3 independent reprogrammings. P values from ANOVA.

Neuron specific expression of MFN2 T105M in mice recapitulates key features of human CMT2A

Children with CMT2A are typically healthy during early years, but develop signs of neuromuscular dysfunction during the mid first decade of life. Neurogenic distal limb muscular atrophy is progressive until the end of the second decade, at which time the disease stabilizes; longevity is normal, but disability is permanent [1,3]. No mouse models of CMT2A recapitulate all of these key clinical features in the absence of confounding developmental phenotypes [15,26-29]. Therefore, a prerequisite for proof-of-concept testing of mitofusin activation *in vivo* was to generate a mouse CMT2A model having greater similarity to the human condition.

By combining Rosa26<fs-$^{MFN2(T105M)}$> [28] and *Mnx1-Cre* (HB9) [30] alleles (**Figure 2a**) we drove human *MFN2* T105M expression in mouse neurons (**Figure 2b**; CMT2A mouse). Neuromuscular functional integrity over time was assessed as the duration mice could walk on an elevated accelerating rotating cylinder without falling off (RotaRod latency). RotaRod latency of CMT2A mice was normal at 10 weeks of age, progressively declined thereafter, and stabilized beyond 30 weeks (**Figure 2c**). As in clinical CMT2A, axonal mitochondria of MFN2 T105M mice were fragmented with disorganized cristae [31] (**Figure 2d**).

Neuroelectrophysiological testing of CMT2A patients characteristically reveals reduced compound motor activation potentials (CMAP) with normal nerve conduction velocities [6,32]. Recapitulating this clinical finding, sciatic nerve-tibialis muscle CMAP amplitudes of 50 week old MFN2 T105M mice were diminished with no change in signal latency, which reflects conduction velocity (**Figure 2e**). Tibialis myofiber atrophy and loss of large axons without demyelination in the MFN2 T015M mouse (*vide infra*) also mimicked clinical CMT2A [22,33,34].

To further evaluate the relevance of the *MFN2* T105M mouse to human CMT2A, dorsal root ganglion (DRG) sensory neurons were isolated and placed in culture, the MFN2 T105M transgene induced with Adeno-Cre, and neurons assayed for the mitochondrial pathologies delineated in reprogrammed CMT2A patient motor neurons (*vide supra*). CMT2A-associated abnormalities in axon mitochondrial aspect ratio and transport (**Figure 2f**) and polarization status (Figure 2 -figure supplement 1) were each mimicked in mouse CMT2A DRGs. As in reprogrammed human CMT2A motor neurons, mitofusin activation improved these abnormalities (**Figure 2f and** Figure 2 -figure supplement 1), compare to Figure 1c)

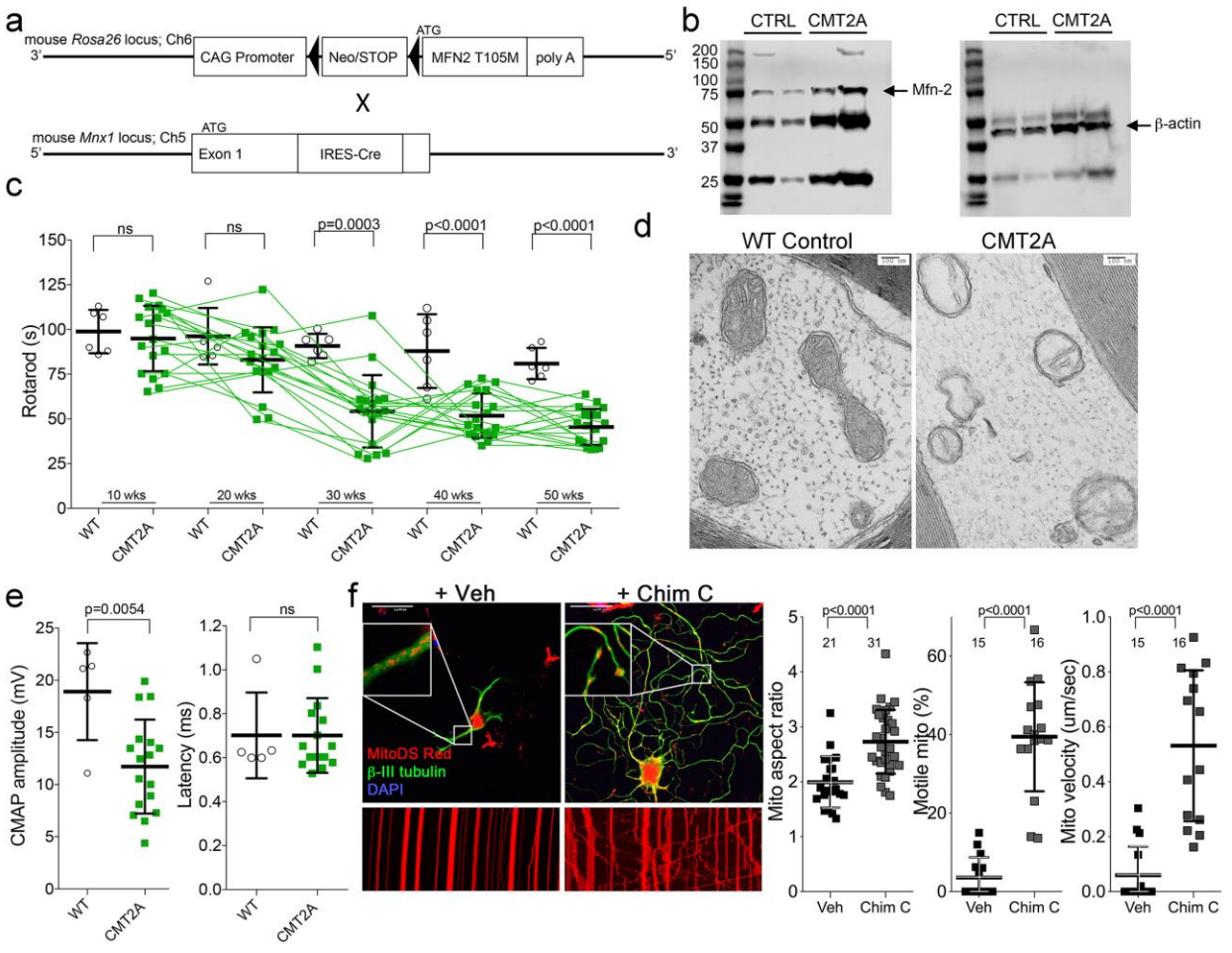

Figure 2. *Characteristics of a neuron-specific MFN2 T105M mouse model of CMT2A.* **a.** Schematic depiction Mfn2 $^{<fs\text{-}T105M>}$ expression strategy. **b.** Immunoblot analysis of MFN2 expression in mouse sciatic nerves. **c.** Serial RotaRod latency studies; CMT2A is green squares (n=16), wild-type (WT) control is open circles (n=6). **d.** Electron micrographs of axonal mitochondrial from sciatic nerves (50 weeks). **e.** Comparative neuro-electrophysiology study results of 50 week old mice in panel c. **f.** Response of CMT2A dorsal root ganglion neurons to mitofusin activation with Chimera C (100 nM, 48 hours). Top images are confocal micrographs of DRGs stained for mitochondria (red) and axons (green). Insets are higher power magnification to see mitochondrial morphology. Bottom images are kymographs showing mitochondrial (red) motility. Vertical columns are stationary mitochondria; lines transiting left to right or right to left are moving. P values are from t-test from 3 or 4 independent experiments.

Burst mitofusin activation reverses neuromuscular dysfunction in CMT2A mice

Collectively, the above results show that activating mitofusins can improve multiple mitochondrial abnormalities manifested by cultured human and mouse CMT2A neurons. To determine whether benefits of mitofusin activation in cultured neurons would translate to therapeutic effects on neuromuscular dysfunction in CMT2A we contemplated an *in vivo* trial in our CMT2A mouse. However, Chimera C is rapidly degraded by the liver and undergoes first-

pass metabolism, making it impractical for *in vivo* studies [25]. We therefore evaluated *in vivo* efficacy of mitofusin activation in CMT2A using MiM111, a structurally distinct compound having a mitofusin activation profile similar to Chimera C (Figure 1 -figure supplement 3), but which is metabolically stable with good nervous system bioavailability [25]. We hypothesized that intermittent or "burst" mitofusin activation (a dosing schedule that reversed mitochondrial dysfunction for <12 hours each day) (Figure 3 -figure supplement 1) would confer therapeutic benefits by cyclically enhancing mitochondrial fitness and transport, while minimizing the possibility of mitofusin toxicity that might occur with constant mitofusin activation[16,35].

Based on a minimum effective MiM111 plasma concentration of 30ng/ml [25] and a plasma $t_{1/2}$ of 2.3 hours with C_{max} of 24,000 ng/ml after intramuscular administration of 30 mg/kg (Figure 3 -figure supplement 1), we estimated that daily IM dosing would reverse mitochondrial dysmotility in CMT2A mice for ~12 hours out of every 24h. Indeed, **Figure 3 -figure supplement 1** show that mitochondrial motility in sciatic nerve axons of MFN2 T105M mice was normalized 4 hours after a single intramuscular injection of MiM111 (30 mg/kg), declined by approximately half after 12 hours, and returned to CMT2A baseline after 24 hours.

If CMT2A neuron die-back is reversible then burst mitofusin activation should improve neuromuscular degeneration in MFN2 T105M mice who had progressed to the severe and stable CMT2A phenotype. To test this notion, 50 week old MFN2 T105M mice and littermate controls were randomized to receive daily MiM111 or its vehicle. Researchers blind to genotype and treatment group performed Rotarod and neuro-electrophysiological testing after 4 and 8 weeks (**Figure 3b**). The characteristic decreases in RotaRod latency and CMAP amplitude in MFN2 T105M mice (see Figures 2c and 2e) were reversed 4 weeks after MiM111 treatment and remained near normal after 8 weeks (**Figures 3c and 3d**); MiM111 had no effect on control mice (Figure 3 -figure supplement 2).

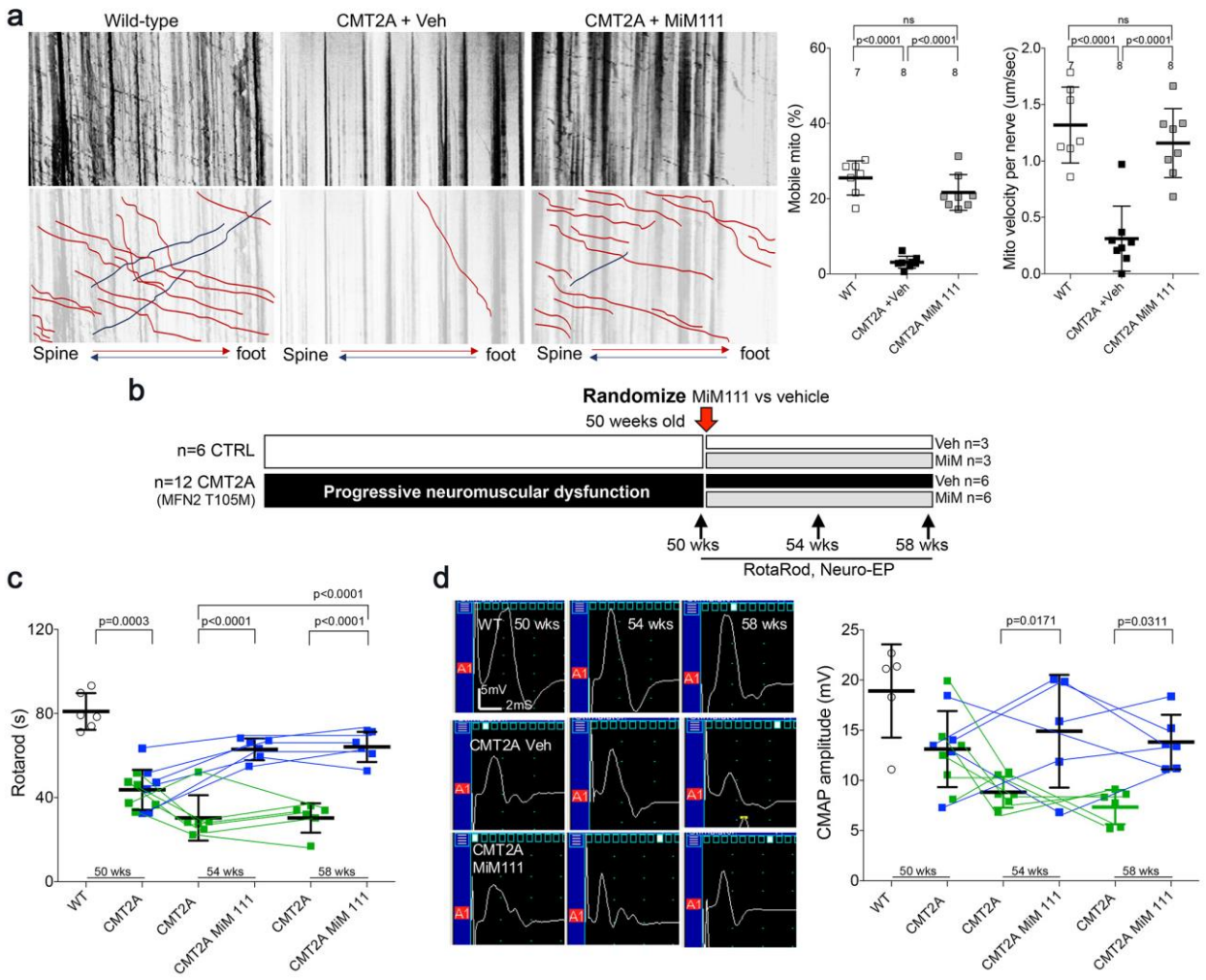

Figure 3. *Mitofusin activation reverses neuromuscular dysfunction in MFN2 T105M mice.* **a.** *Ex vivo* mitochondrial motility in CMT2A mouse sciatic nerve axons 4 hours after intramuscular administration of mitofusin activator MiM111 or vehicle. Top panel is kymographs. Bottom panel emphasize motile mitochondria with red and blue lines transiting antegrade or retrograde, respectively. (Note, mitochondrial transport in *ex vivo* sciatic nerves favors the antegrade [spine to foot] direction because mitochondria are recruited to the site of nerve injury at the distal amputation site [36]. **b.** Experimental design to evaluate efficacy of MiM111 in late murine CMT2A. **c.** RotaRod latency in vehicle- (green) and MiM111-treated (blue) MFN2 T105M mice. **d.** Neuroelectrophysiology studies: (left) representative CMAP tracings; (right) quantitative data. Each symbol in c and d is one mouse. P values from ANOVA. WT control values are open circles in panels c and d; complete WT control data are in Extended Data Fig 6.

Compared to sciatic nerves of vehicle-treated MFN2 T105M CMT2A mice, MiM111 treatment reduced axon damage (**Figure 4a**), increased axon diameter (**Figure 4b**), and increased staining for superior cervical ganglion 10 (SCG10; a marker of neuron regeneration) [37] (**Figure 4**

– figure supplement 1). These findings suggest that mitofusin activation reversed CMT2A-induced neuronal degeneration.

Skeletal myocytes of CMT2A mouse tibialis muscle innervated by the sciatic nerve were abnormally small (**Figure 4c**), reflecting neurogenic muscle atrophy (because the MFN2 T105M transgene is directed by neuron-specific HB9-Cre). In agreement with muscle atrophy being a secondary effect, skeletal myocyte mitochondria of CMT2A mice appeared structurally normal (Figure 4- figure supplement 1) compare to sciatic nerve axon mitochondria in Figs 2d and 4b). Therefore, normalization of tibialis myocyte diameter after mitofusin activation (**Figure 4c**) indicates restoration of neuromuscular integrity.

Collectively, the above findings provide indirect support for the idea that CMT2A mice suffer from distal neuron dieback that can be reversed by activating mitofusins. Reasoning that decreased neuromuscular junction density in CMT2A mice would constitute direct evidence for dieback, we quantified neuromuscular junctional synapses containing receptors for the neurotransmitter acetylcholine (AchR) in tibialis muscles of CMT2A mice. Compared to normal mice, CMT2A mice had ~50% fewer synaptic junctions/myocyte, which was reversed after mitofusin activator treatment (**Figure 4 -figure supplement 1**). Strikingly, mitochondrial occupancy of vehicle-treated CMT2A neuromuscular synaptic junctions was also reduced by ~half compared to normal mice, and was normalized by MiM111 treatment (**Figure 4d**). Because mitochondrial transport can play a central role in neuron repair and regeneration [38], the observation that MiM111 promoted mitochondrial localization within terminal neuromuscular synaptic junctions provided a plausible mechanistic link between mitofusin activation, mitochondrial motility, neuronal regrowth, and reversal of neuromuscular dysfunction in this preclinical CMT2A model.

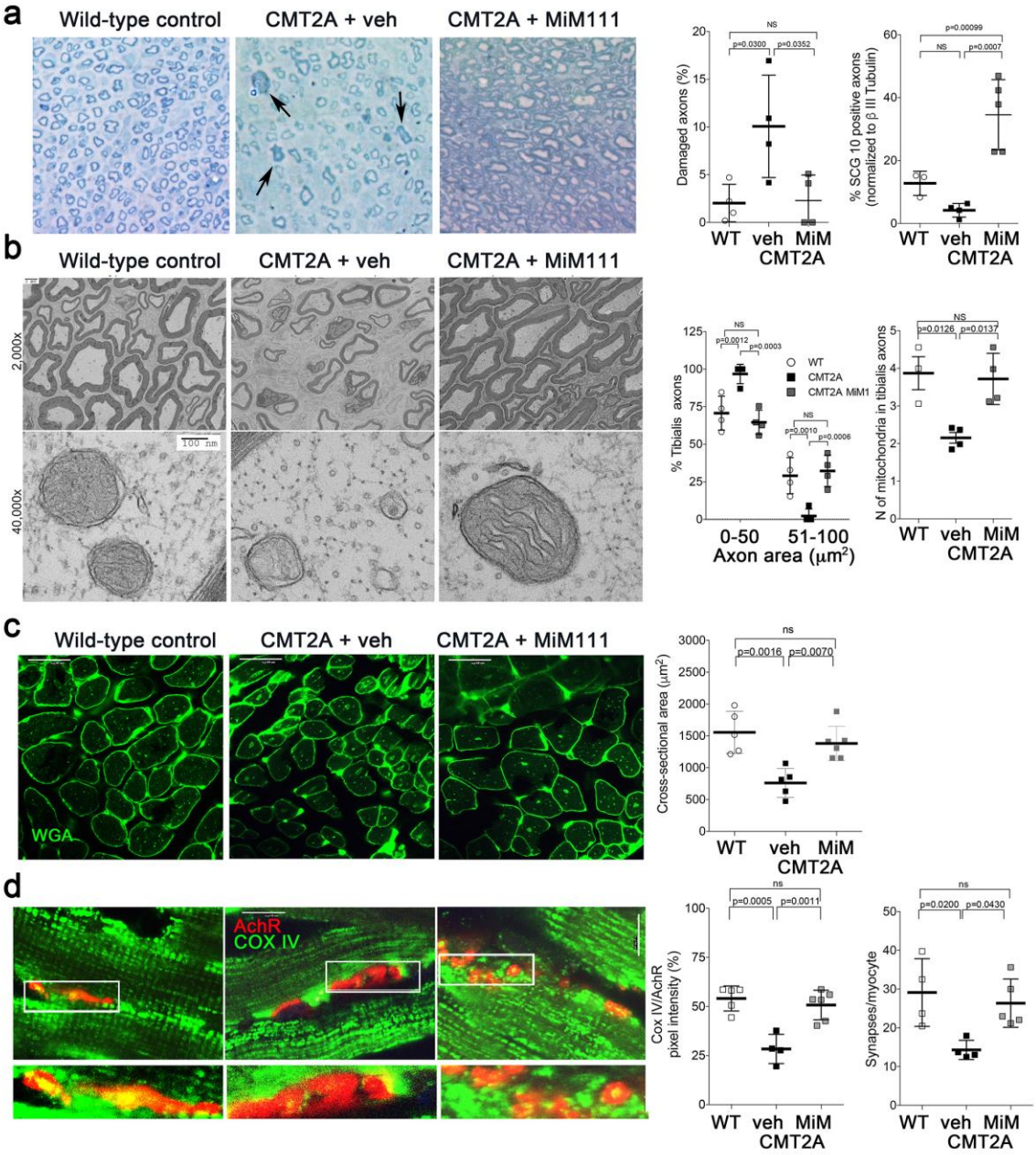

Figure 4. *Mitofusin activation reverses histopathological findings in MFN2 T105M mice.* **a.** Toluidine blue stained sections of mouse mid tibial nerves. Arrows show blue-stained damaged axons in CMT2A mice. Quantitative group data for damaged axons and SCG10-regenerating axons (see Extended Figure 7) are on the right. **b.** Electron micrographs of mid-tibial nerve axons from CMT2A mouse study groups after 8 weeks of therapy. Note heterogeneity in axon size (top images; left graph) and mitochondrial abnormalities (bottom images, right graph). **c.** Wheat germ agglutinin (WGA) labeled sections of tibialis anterior muscle and quantitative myocyte cross sectional area. **d.** Confocal micrographs of neuromuscular junctions to show mitochondrial occupancy yellow organelles within red synapses (also see Extended Data Fig 9). Each symbol represents results from one mouse. Data are means ± SD; p values are 1- or 2-way ANOVA.

Enhanced mitochondrial function in mitofusin-activated CMT2A DRGs leads to accelerated axon growth

Reversal of CMT2A-induced distal neuron die back implies neuronal regrowth. Indeed, sensory DRG neurons isolated from CMT2A mice and cultured in the presence of MiM111 (100 nM, 48 hours) exhibited not only enhanced mitochondrial fusion (increased aspect ratio) and transport (greater mitochondrial motility and velocity), but axon outgrowth (length and branching) (**Figure 5**). Similar effects were seen in CMT2A DRGs treated with Chimera C (100 nM, 48 hours) (Figure 5 -figure supplement 1). Both MiM111 and Chimera C provoked mitochondrial redistribution to axonal termini of cultured CMT2A DRGs (**Figure 5 -figure supplement 1)** recapitulating mitochondrial occupation of neuromuscular synapses after MiM111 treatment of CMT2A mice *in vivo* (see Figure 4d).

Comparing the mitochondrial motility, aspect ratio, and neuron growth responses at different times after mitofusin activation revealed significantly increased mitochondrial trafficking within 2 hours, whereas enhanced axon outgrowth was significant after 24 and 28 hours, and mitochondrial aspect ratio (i.e. fusion) was significant only after 48 hours (**Figure 5 -figure supplement 2**). Given the established role for mitochondrial transport in neuronal repair [38], this temporal sequence lends credence to the idea that accelerated neuron growth is a consequence of enhanced mitochondrial function and redistribution.

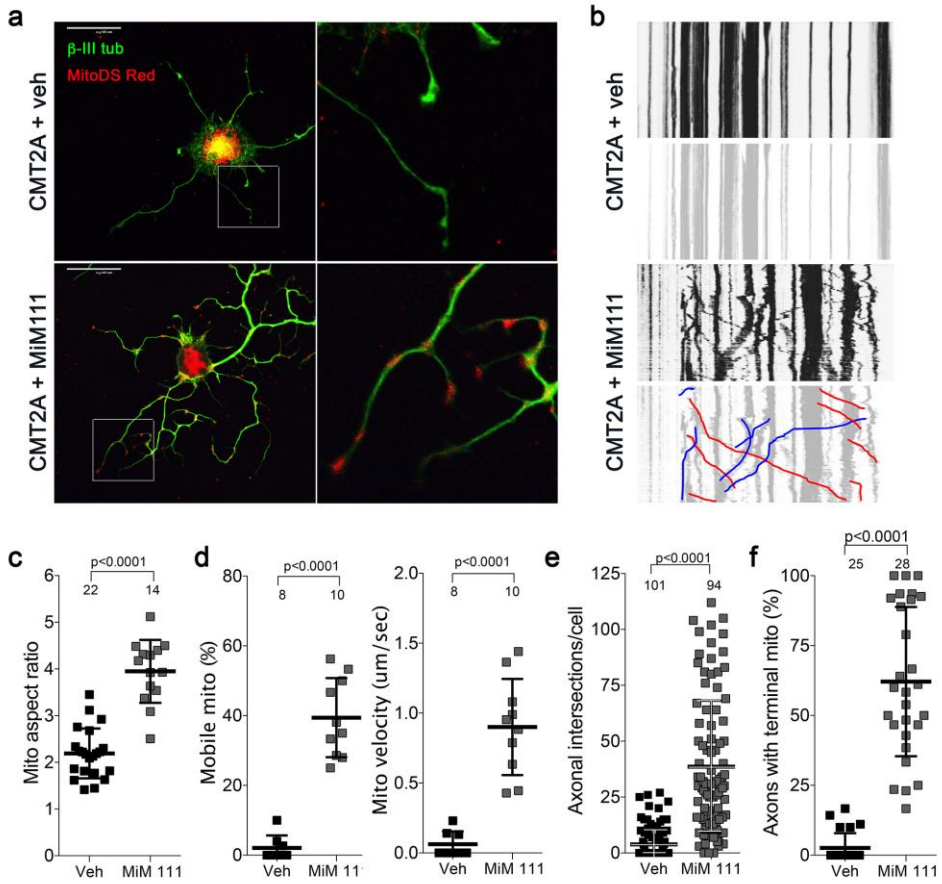

Figure 5. *Mitofusin activation reverses mitochondrial pathology and stimulates growth of CMT2A dorsal root ganglion neurons in vitro.* **a.** Confocal micrographs of CMT2A mouse DRGs cultured for 48h with MiM111 or its vehicle. Note greater neuronal process length and branching in MiM111-treated neuron. Exploded insets (right) show neuronal process termini. Mitochondria express mitoDS Red; neuronal processes stained for β-III tubulin are green. **b.** Kymographs of mitochondrial motility in neuronal processes of live DRGs from studies shown in (a). Top panel is raw data. Bottom panels emphasize motile mitochondria with red and blue lines transiting left to right or right to left, respectively. c-f. Quantitative group data demonstrating effect of MiM111 on CMT2A DRG mitochondrial aspect ratio (c), motility (d, e), neuronal process length and branching (e), and proportion of neuronal process termini containing mitochondria (f).

Mitofusin activation accelerates in vitro CMT2A axon regeneration after axotomy.

DRG outgrowth measures *in vitro* regrowth of neuronal extensions that are amputated during the cell isolation trituration procedure. We considered that a more appropriate model of regrowth after dieback in CMT2A would test intact neurons lacking only the distal axons. Because CMT2A mouse neurons grow poorly in tissue culture in the absence of mitofusin activators (*vide supra*), this was not feasible using DRGs. Therefore, we seeded cortical neurons collected from MFN2 T105M allele mice in chambers separated from empty

chambers by linear microchannels. In the absence of Cre-recombinase these "normal" neurons grew axons through the microchannels that branched into the empty chambers (**Figure 6a**). Adenoviral Cre was then used to activate the CMT2A MFN2 T105M transgene, followed after 48 hours by aspiration amputation of the branched axonal termini (**Figures 6b and 6c**). Mitochondrial motility and aspect ratio were measured 1 hour before and after axotomy; axon regrowth was measured 3 days after axotomy. The aspect ratio of mitochondria in the distal linear axons of normal and CMT2A neurons was unaffected either by axotomy or by MiM111 (**Figure 6d**, left panel). By contrast, and consistent with a previous study in normal neurons [36], mitochondrial motility was reduced by axotomy (**Figure 6d** middle panels). Mitofusin activation with MiM111 after axotomy restored mitochondrial motility and neuronal outgrowth to pre-axotomy levels. Thus, the link between experimentally activating mitofusins, the subsequent increase in mitochondrial transport, and enhanced neuronal growth/repair was consistent for mouse CMT2A sciatic nerve axons *in vivo*, cultured CMT2A DRG neuron outgrowth, and cultured CMT2A cortical nerve regrowth after distal axotomy.

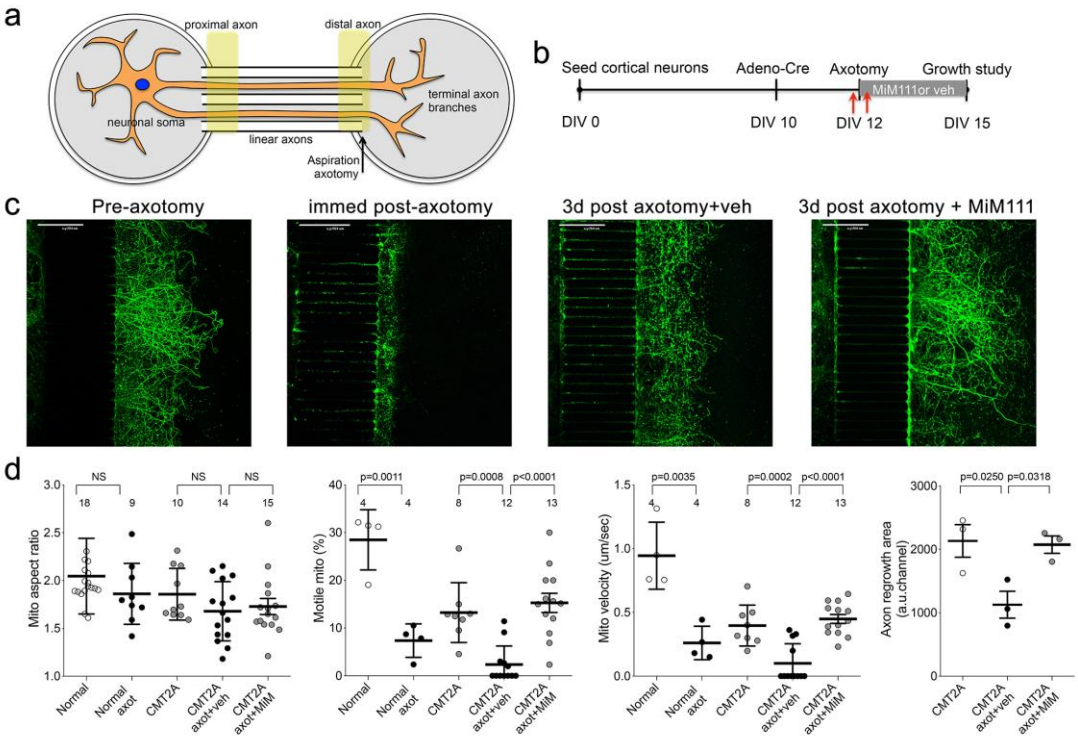

Figure 6. *Mitofusin activation stimulates post-axotomy regrowth of CMT2A cortical neurons in vitro.* **a.** Schematic depiction of microfluidic platform. Yellow areas show proximal axon where mitochondrial motility was measured and distal axon where mitochondrial aspect ratio was measured.

b. Experimental design. DIV is days in vitro. Red arrows are times of pre- and immediate post-axotomy mitochondrial studies. **c.** Representative images of CMT2A neuron terminal branches at different times relative to aspiration axotomy. **d.** Quantitative group data demonstrating effect of MiM111 on CMT2A cortical neuron mitochondrial aspect ratio (left panel), motility (middle panels), and axon length (right panel).

Discussion

These preclinical studies show that activating endogenous normal mitofusins can improve stable neuromuscular dysfunction caused by a CMT2A *MFN2* mutant. Pharmacological mitofusin activation enhanced CMT2A neuron growth *in vivo* and *in vitro* by promoting mitochondrial fitness and transport, thereby reversing CMT2A-associated mitochondrial fragmentation, depolarization and stasis. We believe the key benefit that accrued from directly activating mitofusin-mediated mitochondrial fusion and motility was improved delivery of healthy mitochondria to neuromuscular junctions and axon growth buds. To our knowledge, this is the first report of any experimental intervention that fully reverses *in vivo* CMT2A phenotypes, demonstrating the feasibility of a clinically translatable disease-modifying therapeutic modality for this incurable condition.

Our studies integrated findings from multiple complementary experimental platforms. Motor neurons directly reprogrammed from CMT2A patient fibroblasts have not previously been described, and provided a platform in which effects of therapeutic interventions could be assessed on different patients' mutations and individual genetic backgrounds using a disease-relevant cell type. Compared to iPS cell-derived CMT2A neurons [11,18], direct reprogramming more faithfully reproduced prototypical CMT2A mitochondrial phenotypes. Compared to the parental patient fibroblasts [39], neurons permitted assessment of the CMT2A-associated mitochondrial motility disorders. While CMT2A has both sensory and motor neuropathy components, we reprogrammed specifically for motor neurons because motor components of this disease are the major source of patient disability.

All mouse disease models have advantages and limitations. Our CMT2A mouse model expresses human *MFN2* T105M using a "motor neuron selective" promoter (*vide infra*), and therefore does not exhibit sensory nerve involvement that is sometime manifested in clinical CMT2A. However, compared to other CMT2A mice, the current model more faithfully recapitulates CMT2A neuromuscular dysfunction that is the dominant cause of morbidity in the

human condition [1,3-6]. We previously used young adult mice carrying this combination of MFN2T105M and *HB9*-Cre alleles to evaluate effects of a topically applied prototype mitofusin activator on mitochondrial motility in sciatic nerve axons *ex vivo* [23]. It was not known if, with age, these mice would develop neuromuscular signs similar to clinical CMT2A. As shown here, motor function in these mice is normal at age 10 weeks, but declines until age 30 weeks whereupon it stabilized for at least another 20 weeks. This pattern is similar to the clinical course of CMT2A, in which apparently normal children typically manifest neuromuscular signs in the mid first decade of life, exhibit progressive loss of motor function in distal extremities over the next 10-15 years, and then stabilize. Moreover, the functional (neuroelectrophysiological), histological, and ultrastructural features of axonal tissue in the mice were similar to the human condition. Together with the positive response to mitofusin activation in patient neurons, the improvement in neuromuscular function and cell/organelle pathology in MiM111-treated CMT2A mice supports the approach of mitofusin activation for the clinical disease.

Perhaps the most remarkable finding here is that mitofusin activation reversed the signs of CMT2A in mice with severe, stable disease. Every measured endpoint was improved, including gross neuromuscular function (RotaRod), electrophysiological metrics of neuromuscular integrity (CMAP), read-outs for axon degeneration, and multiple histological and ultrastructural assays of mitochondrial pathology in neurons. *In vivo* and *in vitro* results pointed to enhanced CMT2A neuron repair and regrowth as a central reason for phenotype reversal. Because it is not possible to functionally dissociate mitofusin-mediated increases in mitochondrial fusion and motility, it is unclear if one or the other of these responses preferentially underlies the neuroregenerative effects of mitofusin activation. However, it seems reasonable to postulate that mitochondrial delivery to distal neurons has greatest importance in the long peripheral nerves innervating hands, forearms, feet, and forelegs, i.e. those areas most impacted in CMT2A [1,3-6]. In agreement with this notion, we observed a positive correlation between mitochondrial delivery to or occupancy of axonal termini and CMT2A neuron growth *in vivo* and *in vitro*.

As introduced above, damaging *MFN2* mutations are a straightforward cause of CMT2A, but *MFN2* multifunctionality complicates delineating the underlying cellular pathology [12,29]. For this reason, the specific functional benefits accruing from mitofusin activation in CMT2A cannot unambiguously be defined. Mitochondrial fusion and motility are impaired in CMT2A [9] and

allosteric mitofusin activation corrects both of these parameters [20,23,25]. Mitochondrial respiratory dysfunction, measured here as loss of inner membrane polarization, is a consequence of diminished fusion-mediated homeostatic repair [9], and its improvement can therefore also be explained by enhanced fusogenicity. *MFN2* has a role in mitophagic mitochondrial quality and quantity control [40,41], and allosteric mitofusin activation suppressed the increase in autophagy/mitophagy induced by CMT2A mutant MFN2 T105M in cultured cells [23]. Finally, MFN2 can mediate physical interactions and calcium signaling between mitochondria and endoplasmic reticulum that may also have a role in CMT2A [42], but effects of mitofusin activation on mitochondria-reticular interactions have not been described.

Here, we studied two structurally distinct but functionally similar allosteric mitofusin activators, a new class of drug that is the first to directly enhance mitochondrial fusion and transport. Although the prototype compounds were found not to be "druggable", a new generation of mitofusin activators have addressed pharmaceutical limitations of the initial chemical series [25]. As described previously [23,25], mitofusin activators have minimal effects in normal cells, likely because increasing the probability that mitofusins are in their open/ "active" conformation is a subtle intervention that can be readily compensated for in the absence of a pre-existing imbalance between mitochondrial fusion and fission. The current *in vivo* studies used a short-acting compound administered once daily to evaluate the effects of intermittent, or burst, mitofusin activation on CMT2A neuromuscular dysfunction. We considered that continuous long-term activation of mitochondrial fusion and transport might possibly be deleterious[16] (although it is worth noting that adverse effects of MFN1 and MFN2 overexpression in transgenic mice have not been reported). Moreover, we reasoned that the problem underlying CMT2A is the cumulative effects of long-term mitochondrial stasis and dysfunction on mitochondrial fitness and neuromuscular integrity. This scenario can explain why CMT2A progresses over many years in people and many weeks in mice. Our aim with burst activation was to turn back the disease clock through daily re-setting of mitochondrial function. By intermittently mobilizing healthy mitochondria to distal areas of physiological need, and simultaneously removing senescent or impaired mitochondria, neuron repair, renewal, and neuromuscular signaling were improved.

A mouse is not a man and human neuroregenerative capacity declines with age [43]. For this reason we do not expect that mitofusin activation can fully reverse CMT2A phenotypes in

older human patients with long-term stable disease. Nevertheless, the current results suggest that pharmacological mitofusin activation could offer the first disease-altering therapy for younger CMT2A patients. An intriguing possibility is that mitofusin activation may also have a therapeutic role in some of the many other neurodegenerative conditions not directly caused by mitofusin defects wherein mitochondrial fusion or transport are defective [39,44,45].

Acknowledgements

We gratefully acknowledge helpful discussions with Drs. P. Needleman, P.V. Halushka, and D. Mochly-Rosen, the specialized assistance of L. Zhang., and C. Cantoni for flow cytometry analysis. **Funding:** Supported by NIH R35HL135736, R41NS113642, R41NS115184, Research Grant 628906 from the Muscular Dystrophy Association (GWD), and a McDonnell Center for Cellular and Molecular Neurobiology Postdoctoral Fellowship (AF). G.W.D. is the Philip and Sima K. Needleman-endowed Professor and a Scholar-Innovator awardee of the Harrington Discovery Institute, Videoconfocal and electron microscopy studies were performed at the Washington University Center for Cellular Imaging (WUCCI) supported by the Washington University School of Medicine, the Children's Discovery Institute of Washington University (CDI-COREs 2015-515 and 2019-813) and the Foundation for Barnes-Jewish Hospital (3770 and 4672). **Competing interests:** G.W.D. is an inventor on patent applications PCT/US18/028514 submitted by Washington University and PCT/US19/46356 submitted by Mitochondria Emotion, Inc that cover the use of small molecule mitofusin agonists to treat chronic neurodegenerative diseases, and is a founder of Mitochondria in Motion, Inc., a Saint Louis based biotech R&D company focused on enhancing mitochondrial trafficking and fitness in neurodegenerative diseases. The other authors declare no competing interests. **Data and materials availability:** All data are available in the manuscript or the supplementary material. Studies using MiM111 were performed under terms of an MTA between Mitochondria in Motion, Inc. and Washington University.

References

1. Fridman, V., Bundy, B., Reilly, M.M., Pareyson, D., Bacon, C., Burns, J., Day, J., Feely, S., Finkel, R.S., Grider, T., Kirk, C.A., Herrmann, D.N., Laura, M., Li, J., Lloyd, T., Sumner, C.J., Muntoni, F., Piscosquito, G., Ramchandren, S., Shy, R., Siskind, C.E., Yum, S.W., Moroni, I., Pagliano, E., Zuchner, S., Scherer, S.S. & Shy, M.E. CMT subtypes and disease burden in patients enrolled in the Inherited Neuropathies Consortium natural history study: a cross-sectional analysis. J. Neurol. Neurosurg. Psychiatry 86, 873-878 (2015).
2. Zuchner, S., Mersiyanova, I.V., Muglia, M., Bissar-Tadmouri, N., Rochelle, J., Dadali, E.L., Zappia, M., Nelis, E., Patitucci, A., Senderek, J., Parman, Y., Evgrafov, O., Jonghe, P.D., Takahashi, Y., Tsuji, S., Pericak-Vance, M.A., Quattrone, A., Battaloglu, E., Polyakov, A.V., Timmerman, V., Schroder, J.M. & Vance, J.M. Mutations in the mitochondrial GTPase mitofusin 2 cause Charcot-Marie-Tooth neuropathy type 2A. Nat. Genet. 36, 449-451 (2004).
3. Feely, S.M., Laura, M., Siskind, C.E., Sottile, S., Davis, M., Gibbons, V.S., Reilly, M.M. & Shy, M.E. MFN2 mutations cause severe phenotypes in most patients with CMT2A. Neurology 76, 1690-1696 (2011).
4. Bombelli, F., Stojkovic, T., Dubourg, O., Echaniz-Laguna, A., Tardieu, S., Larcher, K., Amati-Bonneau, P., Latour, P., Vignal, O., Cazeneuve, C., Brice, A. & Leguern, E. Charcot-Marie-Tooth disease type 2A: from typical to rare phenotypic and genotypic features. JAMA Neurol 71, 1036-1042 (2014).
5. Yaron, A. & Schuldiner, O. Common and Divergent Mechanisms in Developmental Neuronal Remodeling and Dying Back Neurodegeneration. Curr. Biol. 26, R628-r639 (2016).
6. Berciano, J., Garcia, A., Gallardo, E., Peeters, K., Pelayo-Negro, A.L., Alvarez-Paradelo, S., Gazulla, J., Martinez-Tames, M., Infante, J. & Jordanova, A. Intermediate Charcot-Marie-Tooth disease: an electrophysiological reappraisal and systematic review. J. Neurol. 264, 1655-1677 (2017).
7. Beręsewicz, M., Charzewski, Ł., Krzyśko, K.A., Kochański, A. & Zabłocka, B. Molecular modelling of mitofusin 2 for a prediction for Charcot-Marie-Tooth 2A clinical severity. Sci. Rep. 8, 16900 (2018).
8. Chan, D.C. Fusion and fission: interlinked processes critical for mitochondrial health. Annu. Rev. Genet. 46, 265-287 (2012).
9. Chen, H. & Chan, D.C. Critical dependence of neurons on mitochondrial dynamics. Curr. Opin. Cell Biol. 18, 453-459 (2006).
10. Pareyson, D., Saveri, P., Sagnelli, A. & Piscosquito, G. Mitochondrial dynamics and inherited peripheral nerve diseases. Neurosci. Lett. 596, 66-77 (2015).
11. Rizzo, F., Ronchi, D., Salani, S., Nizzardo, M., Fortunato, F., Bordoni, A., Stuppia, G., Del Bo, R., Piga, D., Fato, R., Bresolin, N., Comi, G.P. & Corti, S. Selective mitochondrial depletion, apoptosis resistance, and increased mitophagy in human Charcot-Marie-Tooth 2A motor neurons. Hum. Mol. Genet. 25, 4266-4281 (2016).
12. Filadi, R., Pendin, D. & Pizzo, P. Mitofusin 2: from functions to disease. Cell Death Dis. 9, 330 (2018).

13. Baloh, R.H., Schmidt, R.E., Pestronk, A. & Milbrandt, J. Altered axonal mitochondrial transport in the pathogenesis of Charcot-Marie-Tooth disease from mitofusin 2 mutations. J. Neurosci. 27, 422-430 (2007).
14. Crunkhorn, S. Neurodegenerative disorders: Rescuing mitochondrial motility. Nat Rev Drug Discov 17, 391 (2018).
15. Zhou, Y., Carmona, S., Muhammad, A., Bell, S., Landeros, J., Vazquez, M., Ho, R., Franco, A., Lu, B., Dorn, G.W., 2nd, Wang, S., Lutz, C.M. & Baloh, R.H. Restoring mitofusin balance prevents axonal degeneration in a Charcot-Marie-Tooth type 2A model. J. Clin. Invest. 130, 1756-1771 (2019).
16. El Fissi, N., Rojo, M., Aouane, A., Karatas, E., Poliacikova, G., David, C., Royet, J. & Rival, T. Mitofusin gain and loss of function drive pathogenesis in Drosophila models of CMT2A neuropathy. EMBO Rep 19(2018).
17. Stuppia, G., Rizzo, F., Riboldi, G., Del Bo, R., Nizzardo, M., Simone, C., Comi, G.P., Bresolin, N. & Corti, S. MFN2-related neuropathies: Clinical features, molecular pathogenesis and therapeutic perspectives. J. Neurol. Sci. 356, 7-18 (2015).
18. Saporta, M.A., Dang, V., Volfson, D., Zou, B., Xie, X.S., Adebola, A., Liem, R.K., Shy, M. & Dimos, J.T. Axonal Charcot-Marie-Tooth disease patient-derived motor neurons demonstrate disease-specific phenotypes including abnormal electrophysiological properties. Exp. Neurol. 263, 190-199 (2015).
19. Abernathy, D.G., Kim, W.K., McCoy, M.J., Lake, A.M., Ouwenga, R., Lee, S.W., Xing, X., Li, D., Lee, H.J., Heuckeroth, R.O., Dougherty, J.D., Wang, T. & Yoo, A.S. MicroRNAs Induce a Permissive Chromatin Environment that Enables Neuronal Subtype-Specific Reprogramming of Adult Human Fibroblasts. Cell Stem Cell 21, 332-348.e339 (2017).
20. Franco, A., Kitsis, R.N., Fleischer, J.A., Gavathiotis, E., Kornfeld, O.S., Gong, G., Biris, N., Benz, A., Qvit, N., Donnelly, S.K., Chen, Y., Mennerick, S., Hodgson, L., Mochly-Rosen, D. & Dorn, G.W., II. Correcting mitochondrial fusion by manipulating mitofusin conformations. Nature 540, 74-79 (2016).
21. Crowley, L.C., Christensen, M.E. & Waterhouse, N.J. Measuring Mitochondrial Transmembrane Potential by TMRE Staining. Cold Spring Harb Protoc 2016(2016).
22. Verhoeven, K., Claeys, K.G., Zuchner, S., Schroder, J.M., Weis, J., Ceuterick, C., Jordanova, A., Nelis, E., De Vriendt, E., Van Hul, M., Seeman, P., Mazanec, R., Saifi, G.M., Szigeti, K., Mancias, P., Butler, I.J., Kochanski, A., Ryniewicz, B., De Bleecker, J., Van den Bergh, P., Verellen, C., Van Coster, R., Goemans, N., Auer-Grumbach, M., Robberecht, W., Milic Rasic, V., Nevo, Y., Tournev, I., Guergueltcheva, V., Roelens, F., Vieregge, P., Vinci, P., Moreno, M.T., Christen, H.J., Shy, M.E., Lupski, J.R., Vance, J.M., De Jonghe, P. & Timmerman, V. MFN2 mutation distribution and genotype/phenotype correlation in Charcot-Marie-Tooth type 2. Brain 129, 2093-2102 (2006).
23. Rocha, A.G., Franco, A., Krezel, A.M., Rumsey, J.M., Alberti, J.M., Knight, W.C., Biris, N., Zacharioudakis, E., Janetka, J.W., Baloh, R.H., Kitsis, R.N., Mochly-Rosen, D., Townsend, R.R., Gavathiotis, E. & Dorn, G.W., 2nd. MFN2 agonists reverse mitochondrial defects in preclinical models of Charcot-Marie-Tooth disease type 2A. Science 360, 336-341 (2018).

24. Detmer, S.A. & Chan, D.C. Complementation between mouse Mfn1 and Mfn2 protects mitochondrial fusion defects caused by CMT2A disease mutations. J. Cell Biol. 176, 405-414 (2007).
25. Dang, X., Zhang, L., Franco, A., Li, J., Rocha, A.G., Devanathan, S., Dolle, R.E., Bernstein, P.R. & Dorn, G.W., II. Discovery of 6-Phenylhexanamide Derivatives as Potent Stereoselective Mitofusin Activators for the Treatment of Mitochondrial Diseases. J. Med. Chem. 63, 7033-7051 (2020).
26. Detmer, S.A., Vande Velde, C., Cleveland, D.W. & Chan, D.C. Hindlimb gait defects due to motor axon loss and reduced distal muscles in a transgenic mouse model of Charcot-Marie-Tooth type 2A. Hum. Mol. Genet. 17, 367-375 (2008).
27. Cartoni, R., Arnaud, E., Medard, J.J., Poirot, O., Courvoisier, D.S., Chrast, R. & Martinou, J.C. Expression of mitofusin 2(R94Q) in a transgenic mouse leads to Charcot-Marie-Tooth neuropathy type 2A. Brain 133, 1460-1469 (2010).
28. Bannerman, P., Burns, T., Xu, J., Miers, L. & Pleasure, D. Mice Hemizygous for a Pathogenic Mitofusin-2 Allele Exhibit Hind Limb/Foot Gait Deficits and Phenotypic Perturbations in Nerve and Muscle. PLoS One 11, e0167573 (2016).
29. Dorn, G.W., 2nd. Mitofusin 2 Dysfunction and Disease in Mice and Men. Front. Physiol. 11, 782 doi: 710.3389/fphys.2020.00782 (2020).
30. Yang, X., Arber, S., William, C., Li, L., Tanabe, Y., Jessell, T.M., Birchmeier, C. & Burden, S.J. Patterning of muscle acetylcholine receptor gene expression in the absence of motor innervation. Neuron 30, 399-410 (2001).
31. Sole, G., Ferrer, X., Vital, C., Martin-Negrier, M.L., Vital, A. & Latour, P. Ultrastructural mitochondrial modifications characteristic of mitofusin 2 mutations (CMT2A). J. Peripher. Nerv. Syst. 14, 206-207 (2009).
32. Harding, A.E. & Thomas, P.K. The clinical features of hereditary motor and sensory neuropathy types I and II. Brain 103, 259-280 (1980).
33. Muglia, M., Zappia, M., Timmerman, V., Valentino, P., Gabriele, A.L., Conforti, F.L., De Jonghe, P., Ragno, M., Mazzei, R., Sabatelli, M., Nicoletti, G., Patitucci, A.M., Oliveri, R.L., Bono, F., Gambardella, A. & Quattrone, A. Clinical and genetic study of a large Charcot-Marie-Tooth type 2A family from southern Italy. Neurology 56, 100-103 (2001).
34. Neves, E.L. & Kok, F. Clinical and neurophysiological investigation of a large family with dominant Charcot-Marie-Tooth type 2 disease with pyramidal signs. Arq. Neuropsiquiatr. 69, 424-430 (2011).
35. Meyer, J.N., Leuthner, T.C. & Luz, A.L. Mitochondrial fusion, fission, and mitochondrial toxicity. Toxicology 391, 42-53 (2017).
36. Zhou, B., Yu, P., Lin, M.Y., Sun, T., Chen, Y. & Sheng, Z.H. Facilitation of axon regeneration by enhancing mitochondrial transport and rescuing energy deficits. J. Cell Biol. 214, 103-119 (2016).
37. Shin, J.E., Geisler, S. & DiAntonio, A. Dynamic regulation of SCG10 in regenerating axons after injury. Exp. Neurol. 252, 1-11 (2014).
38. Sheng, Z.H. The Interplay of Axonal Energy Homeostasis and Mitochondrial Trafficking and Anchoring. Trends Cell Biol. 27, 403-416 (2017).
39. Dang, X., Rifai, K., Walton, E.K., Zablocka, B., Baloh, R.H., Shy, M.E, Mochly-Rosen, D., Devanathan, S., & Dorn, G.W., 2nd. Mitochondrial phenotypes in genetically diverse

neurodegenerative diseases and their response to mitofusin activation. eLife submitted as companion eLife Research Advance.
40. Chen, Y. & Dorn, G.W., 2nd. PINK1-phosphorylated mitofusin 2 is a Parkin receptor for culling damaged mitochondria. Science 340, 471-475 (2013).
41. Gong, G., Song, M., Csordas, G., Kelly, D.P., Matkovich, S.J. & Dorn, G.W., 2nd. Parkin-mediated mitophagy directs perinatal cardiac metabolic maturation in mice. Science 350, aad2459 (2015).
42. Larrea, D., Pera, M., Gonnelli, A., Quintana-Cabrera, R., Akman, H.O., Guardia-Laguarta, C., Velasco, K.R., Area-Gomez, E., Dal Bello, F., De Stefani, D., Horvath, R., Shy, M.E., Schon, E.A. & Giacomello, M. MFN2 mutations in Charcot-Marie-Tooth disease alter mitochondria-associated ER membrane function but do not impair bioenergetics. Hum. Mol. Genet. 28, 1782-1800 (2019).
43. Mattson, M.P. & Magnus, T. Ageing and neuronal vulnerability. Nat. Rev. Neurosci. 7, 278-294 (2006).
44. Knott, A.B., Perkins, G., Schwarzenbacher, R. & Bossy-Wetzel, E. Mitochondrial fragmentation in neurodegeneration. Nat. Rev. Neurosci. 9, 505-518 (2008).
45. Burte, F., Carelli, V., Chinnery, P.F. & Yu-Wai-Man, P. Disturbed mitochondrial dynamics and neurodegenerative disorders. Nat. Rev. Neurol. 11, 11-24 (2015).
46. Sobieski, C., Jiang, X., Crawford, D.C. & Mennerick, S. Loss of Local Astrocyte Support Disrupts Action Potential Propagation and Glutamate Release Synchrony from Unmyelinated Hippocampal Axon Terminals In Vitro. J. Neurosci. 35, 11105-11117 (2015).
47. Schneider, C.A., Rasband, W.S. & Eliceiri, K.W. NIH Image to ImageJ: 25 years of image analysis. Nat Methods 9, 671-675 (2012).

Materials and Methods

Mouse lines

Rosa-STOP-mMFN Thr105Met (T105M) mice (C57BL/6 Gt(ROSA)26 Sortm1 (CAG-*MFN2**T105M)Dple/J) from The Jackson Laboratory (Bar Harbor, Maine, USA; Stock No: 025322, RRID:MGI:_JAX:025322) were crossed to HB9-Cre mice (B6.129S1-Mnx1tm4(cre)Tmj/J) from The Jackson Laboratory (Stock No: 006600, RRID:MGI:_JAX:006600)) to generate neuron-targeted MFN2 T105M mice. HB9 is a motoneuron-specific promoter [30], but JAX data indicates that this HB9-Cre line also drives expression in some sensory DRG neurons (https://images.jax.org/webclient/img_detail/20564/). All experimental procedures were approved by Washington University in St. Louis School of Medicine Animal Studies Committee; IACUC protocol number 19-0910, Exp:12/16/2022.

Cell lines

Normal mouse embryonic fibroblasts (MEFs) were prepared by enzymatic dissociation from embryonic day E.13.5-14.5 C57BL/6J mice (The Jackson Laboratory Cat:# 000664, RRID:IMSR_JAX:000664). *Mfn1* null and *Mfn2* null *Mfn1/Mfn2* double null MEFs fibroblasts were purchase from American Type Culture Collection (ATCC Manassas, Virginia, USA) (CRL-2992, RRID:CVCL_L691 and CRL-2994, RRID:CVCL_L692 and CRL-2993, RRID:CVCL_L693 respectively). Human fibroblast: Dermal fibroblast (MFN2 T105M) and Dermal fibroblast (MFN2 H361Y) from Dr. Robert H. Baloh (Cedars Sinai), Dermal fibroblast (MFN2 R274W) from Dr. Barbara Zablocka (Mossakowski Med Res Ctr), Dermal fibroblast (MFN2 R364W) from Dr. Michael E. Shy (University of Iowa). Dermal fibroblast (Normal) from NINDS respectively : ND34769, RRID:CVCL_EZ04, ND36320, RRID:CVCL_EZ16 and ND29510, RRID:CVCL_Y813)
.

Viral vectors

Adenovirus expressing human FLAG-hMFN2 -T105M was prepared at Vector Biolabs (Malvern, PA, USA). Adenoviri expressing β-galactosidase (Ad-CMV-β-Gal; #1080), and Ad-Cre (#1794) were purchased from Vector Biolabs. Adenovirus for Mito-Ds-Red2 came from Signagen (Cat:#SL1007744) . Lentivirus packaging vectors: psPAX2 (Addgene, Cat#: 12260) pMD2.G (Addgene, Cat#: 12259), Lentiviral vectors with recombinant DNA: rtTA-N144 (Addgene, Cat#: 66810) pTight-9-124-BclxL (Addgene, Cat#: 60857), human LHX3-N174 and human ISL1-N174 were packaged and used as described [19].

Antibodies

Mouse monoclonal anti-mitofusin 2 (Cat # ab56889 - 1:1000, RRID:AB_2142629), anti-COX-IV (Cat #ab16056 - 1:1000, RRID:AB_443304) and anti-GAPDH (Cat #ab8245 - 1:1000, RRID:AB_2107448) were from AbCAM (Cambridge, MA, USA). Rabbit polyclonal anti-Stathmin-2/Superior Cervical Ganglion 10 (SCGN10; Cat # NBP1-4946, RRID:AB_10011569) was from Novus Biologicals (Littleton, CO, USA).Rabbit polyclonal FSP-1 was from Sigma Millipore (Cat # 07-2274, RRID:AB_10807552). Anti-mouse monoclonal -MNX1was from DSHB (1:10, Cat# 81.5C10, RRID:AB_2145209). Mouse monoclonal anti-β -tubulin III (Cat # 801201- 1:500, RRID:AB_2313773) was from Biolegend

(San Diego, CA, USA). Peroxidase-conjugated anti-mouse IgG (Cat #7076S - 1:1000, RRID:AB_330924) was from Cell Signaling (Danvers, MA, USA). Goat anti-rabbit IgG (Spicier reactivity Goat, Host/Isotype Rabbit/IgG; Cat #31460, RRID:AB_228341) and Alexa-Fluor 488 anti-mouse ThermoFisher (Waltham, MA, USA Cat #A11008, RRID:AB_143165). α-Bugarotoxin Alexa flour 594 was from ThermoFisher, Waltham, MA, USA Cat:# B12423.

PCR genotyping of MFN2 mutations in CMT2A patient fibroblasts

DNA was extracted from 5 x 10^6 primary human fibroblasts using the DNeasy blood & tissue kit (Qiagen, Cat#: 69506) according to manufacturer's protocol. PCR used Taq Plus Master Mix 2X (Cat#: BETAQR-L, Bulls eye). 50 ng of genomic DNA template, and the following primers:

(*MFN2* T105M) - 5'- TTGCACTGAATAGGGCTTTG- 3'
5'- CATTCACCTCCACAGGGTG- 3'
(*MFN2* R274W) - 5'- CGTGGTAGGTGTCTACAAGAAGC- 3'
5'- CTGGTGAGGGCTGATGAAAT- 3'
(*MFN2* H361Y, R364W) - 5'-CCTGGCAGTGAAAACCAGAG- 3'
5'- AAGGCGTGTCCTAACTGCC- 3'.

PCR products were purified using PureLink Quick Gel Extraction Kit (Cat#: K21000-12, Invitrogen). Sanger sequencing of PCR products was performed at GENEWIZ.

Cultured cells

Direct reprogramming of human motor neurons from patient fibroblasts used the procedure as described [19]. Reprogramming cocktail consisted of 1 mL concentrated lentivirus containing the reverse tetracycline-controlled transactivator (rtTA; Addgene, Cat# 66810), 1 ml virus containing pT-BclXL-9/9*-124, 125ul virus containing motor neuron transcription factor ISL1, and 125ul virus containing motor neuron transcription factor LHX3 with polybrene (8 μg/mL; Sigma-Aldrich, Cat# H9268). Human skin fibroblasts of low passage number (P4-P7) were spinfected at 37°C for 30 minutes at 1,000×G. Doxycycline (Dox, 1 ug/mL; Sigma Aldrich, Cat# D9891) and antibiotics for respective vectors (Puromycin, 3ug/mL; Invitrogen, Cat# A11138-03; Geneticin, 400 ug/mL; Invitrogen, Cat# 10131-035) were added to culture medium for four days after viral transduction. On day 5 cells were re-plated on poly-ornithine/laminin/fibronectin (Sigma, Cat# P4957, # L2020, # F4759) coated 18mm glass coverslips and on the following day changed to neuronal medium supplemented with Dox (1ug/ml added every other day), valproic acid (1 mM; Sigma, Cat# 676380), dibutyryl cAMP (200 uM; Sigma, Cat# D0627), BDNF, NT-3, CNTF, GDNF (all 10 ng/mL, Peprotech, Cat# 450-02, #450-03, #450-13, #450-10), retinoic Acid (1 uM; Sigma, Cat# R2625) and antibiotics. Neuronal media was refreshed by replacing half every 4 days. Antibiotics were discontinued on day 14; Dox was discontinued on day 30. Cells underwent studies beginning on day 35. Motor neurons were identified after formalin fixation by labeling with mouse anti-MNX1 (1:10; DSHB, Cat# 81.5C10) and mouse anti-TUBB3B (1:2000; Biolegend, Cat#PRB-435P-100). Fibroblasts were identified by labeling with rabbit anti FSP-1 (1:200; Sigma, Cat: # 07-2274).

Adult mouse dorsal root ganglion (DRG) neurons were prepared from ~ 8 week-old HB9Cre-MFN2 Thr105Met flox-stop transgenic mice as previously described [23]. To comprehensively induce MFN2 T105M transgene expression, the DRGs were infected with Adeno-Cre (M.O.I. of

50) 48h prior to study. DRG neurons were distinguished from non-neuronal cells by staining with anti-β-III tubulin.

Mouse cortical neurons were isolated from individual embryonic day E.18.5 MFN2 Thr105Met flox-stop transgenic mice by papain digestion and mechanical dispersion using a published procedure [46]. Briefly, mouse brain cortices were isolated under a dissecting microscope and sliced into 0.5-1 mm thick sections in Leibovitz's L-15 Medium (Gibco Cat:#11415-064) containing BSA (0.23mg/ml, Sigma Cat:#A7030). Papain (1mg/ml, Sigma Cat #P4762) was added and the tissue digested for 20 min at 37°C. The papain solution was replaced and micropipettes used to triturate the solution until no more tissue was visible. Cortical neurons were plated in microfluidic neuron XonaChip chambers as described below.

Imaging

Static confocal imaging of cultured neurons used triple-stained with MitoTracker Green (200 nM; Invitrogen, Thermo Fisher Scientific Cat:# M7514) to visualize mitochondria, tetramethylrhodamine ethyl ester (TMRE, 200 nM, Invitrogen Thermo Fisher Scientific Cat:# T-669) that labels mitochondria with normal polarization of the mitochondrial inner membrane, and Hoechst (10 μg/ml; Invitrogen, Thermo Fisher Scientific Cat:# H3570) that stains nuclei blue as described [20]. Static live cell images were acquired on a Nikon Ti Confocal microscope using either a 60X1.3 NA oil- immersion objective or 10X0.3 NA dry objective, in Krebs-Henseleit buffer (138 NaCl, 3.7 nM KCL, 1.2 n M KH2PO4, 15 nM Glucose, 20 nM HEPES pH: 7.2-7.5, and 1mM CaCl2): laser excitation was 488 nm with emission at 510 nm for MitoTracker Green and Ad-Mito GFP, 549 nm with emission at 590 nm for TMRE, and 306 nm with emission 405 nm for Hoecsht and DAPI.

Axon branching analysis of CMT2A mouse DRGs was performed at various times after isolation and plating, as indicated. In some studies neurons were infected with Ad-mito-RFP to label mitochondria red. Cells were fixed and labeled with anti-β-tubulin III (1:200 in 10% goat serum in PBS) to identify neurons. Images were acquired using the 10x objective and excitation at 488 nm/emission 510 nm for Alexa-Flour 488 and 579 excitation/599 emission for mito-RFP. Sholl analysis of axonal branching used ImageJ [47] and an open source plugin (https://imagej.net/Sholl_Analysis). Briefly, a starting radius was set to encompass the soma of β-tubulin III-positive DRG neurons and concentric circles established at 10 micron increments, to 40 microns. Numbers of axon and radii intersections were totaled for all circles to derive intersection number, which is a measure of axonal branching. Special attention was given to ensure that there was uniform staining along all parts of the DRG soma and axons so that the plugin was able to accurately assess the number of intersections accurately.

Video confocal studies of mitochondrial motility studies in neurons and sciatic nerves used time-lapse imaging (1 frame every 5 seconds) for 121 frames (10 minutes, sciatic nerve) or 180 frames (15 minutes, cultured neurons) at 37 degrees C on a Nikon A1Rsi Confocal Microscope using a 40x oil objective as described [23]. Cultured neuron mitochondria were labeled with Adeno-mitoDsRed2 or MitoTracker Orange (200 nM, Invitrogen Thermo Fisher Scientific Cat:# M7510) excited at 561 nm, emission 585nm. Sciatic nerve axon mitochondria were labeled with TMRE. Kymographs and quantitative data were generated using an Image-J plug-in.

In vitro microfluidic studies of axon growth used primary cortical neurons isolated from embryonic day 18.5 MFN2 T105M flox-stop mice. 50,000 – 90,000 suspended cells in 20 µl of Earle's Minimal Essential Medium (MEM; #11090-081; Gibco) supplemented with 5% FBS (Gibco #16140-063), 5% horse serum (HS) (Gibco #26050-070), 400µM L-Glutamine (Gibco #25030-149), 50 units/ml each penicillin/streptomycin (Gibco #15070-063) and 0.3% glucose (Sigma G 5767) (5-5 media) was added to the left chambers of XonaChips with 450 µm microgroove barriers (#XC450; Xona Microfluidics, Temecula, CA, USA) coated with 0.5mg/ml poly(D)lysine (Sigma #P7280). Ten minutes therafter, 150µl of 5-5 media supplemented with 0.5µl Insulin-Transferrin-Sodium Selenite (Sigma I 1884) was added to each well and neurons cultured under standard conditions. After 24 hours the media was changed to Neurobasal Media (#21103-049; Gibco, Carlsbad, CA, USA), 1x B27 Supplement (#17504-044, Gibco, Carlsbad, CA, USA), 50 units/ml each Penicillin/Streptomycin (#15070-063; Gibco, Carlsbad, CA, USA) and 400µM L-Glutamine (#25030-149; Gibco, Carlsbad, CA, USA) with feeding every 2 to 3 days until axotomy (DIV 12), and infected with adeno-Cre for 48 hours to induce MFN2 Thr105Met expression. Vacuum aspiration axotomy and post-axotomy regrowth analyses were performed as described [36]. Aspiration axotomy was followed by application of fresh neuron feeding media containing MIM111 (100 nM) or its vehicle (Me_2SO, 1:1,000). Cells were fixed in situ; axonal outgrowth and post-axotomy regrowth were analyzed by confocal analysis of β-III tubulin positive cells. The area of βIII-tubulin signals above the same threshold within a 1024 × 1024 image that covers all axon segments extending from microgrooves was measured using ImageJ (NIH) and reported as pixels density of axon segments extending from an average of all microgrooves.

Immunoblot analysis was performed on mouse sciatic nerve proteins size-separated on 10% SDS-PAGE gels (Biorad Cat# 456-1036) and transferred to 0.45µM Polyvinylidene fluoride (PVDF) membranes (GE- Amersham, Freiburg, Germany Cat# 10600023). Membranes were blocked with 5% non-fat milk for 30 minutes and incubated with primary antibody overnight at 4˚C. Peroxidase-conjugated secondary antibodies and Chemiluminescence Substrate (Thermo Scientific #32132) were used for signal detection. Quantification of immunoreactive proteins was performed on a LI-COR Odyssey infrared detection system (Lincoln, NE, USA, version 1.0.17).

Flow cytometric analysis of mitochondrial electrochemical potential

Cultured neurons were stained *in situ* with TMRE (200 nM, Invitrogen Thermo Fisher Scientific Cat:# T-669) for 30 min at 37°C in 5% CO2-95% air, washed twice in PBS, and released from culture substrates with 0.05% Trypsin-EDTA (Gibco, cat:# 1995647). After centrifugation, the DRG pellets were re-suspended in 200 ul of FACS buffer (PBS 1X, BSA 1X, 2Mm EDTA). Flow cytometry of TMRE fluorescence was performed on a Gallios instrument (Beckman Coulter) and analyzed using FlowJo10 software. ~3500 events were acquired for each sample. Data are presented as Mean Fluorescence Intensity per experiment. In some studies carbonyl cyanide-*p*-trifluoromethoxyphenylhydrazone (FCCP, 10 µM for 1 h) (Sigma, Cat #C2759) was added as a positive control for mitochondrial depolarization.

Evaluation of neuromuscular phenotypes in CMT2A mice

Rotarod studies were performed on mice initially acclimated to the RotaRod (Ugo Basile, Gemonio, VA, Italy;# 47650) at a speed of 5 r.p.m. CMT2A mice underwent RotaRod

evaluations weekly from 10-50 weeks for disease development, and 4 and 8 weeks after mitofusin activator therapy. The acceleration protocol increased from 5 to 40 r.p.m over 120 seconds and then maintained 40 r.p.m. indefinitely. Each mouse underwent 5 separate trials per testing event with 5 min rest between trials. Latency (time to falling off) was averaged for all trials.

Neuroelectrophysiologic recordings of tibialis/gastrocnemius compound muscle action potentials (CMAP) were performed with a Viasys Healthcare Nicolet Biomedical instrument (Middleton, WI, USA Cat:# OL060954) running Viking Quest version 11.2 software by an operator (A.F.) blinded to genotype and treatment group. Mice were anesthetized with isofluorane (4-5% induction, 1.5% maintenance), shaved, and the proximal sciatic nerves stimulated using a needle electrode (Natus, Mundelein, IL, USA Cat:# F-E2-48) with 3.9 mV pulses of 0.002 ms duration. Ring electrodes (Natus, Mundelein, IL, USA Cat:# 291965) were positioned at the mid forelimb at the belly of the tibialis anterior and gastrocnemius muscles to record CMAP. Optimal stimulating electrode position was determined as that giving the greatest CMAP amplitude; 3-4 independent events were recorded and averaged.

Evaluation of CMT2A mouse responses to MiM111

Twelve 50 week old CMT2A mice (HB9-Cre + MFN2 Thr105Met flox-stop) and 6 littermate controls were randomized and blinded to daily intramuscular treatment with MiM111 or vehicle for 8 weeks: under sterile conditions18.75 mg/ml (64.8mM) MIM 111 was dissolved in 10% Me_2SO/90% (2-hydroxypropyl)-β-cyclodextrin (HP-BCD; Sigma, Cat :#332607), sterile-filtered (0.22μm PVDF, #SLGV033RS, Millipore, Cork, Ireland), and drug- or vehicle-containing syringes were assigned to individual mice by XD using a randomization table. Daily intramuscular injections (biceps femoris muscle, alternating left and right every other day) were performed by AF, who was blinded to both mouse genotype and drug treatment group. Rotarod and neurophysiological testing were performed before, and 4 and 8 weeks after initiation of therapy. Mice were terminated by anesthesia overdose after 8 weeks for tissue studies. Sciatic and mid tibial nerves were dissected from both legs of all mice. For histology and immunohistology the left leg nerves or muscles were fixed in PFA for 2 hours, transferred to 30% sucrose/PBS overnight at 4 degrees C, and embedded in optimal cutting temperature (OCT, Tissue-TEK Cat: 4583) medium for storage at -80 degrees C. Immunostaining with anti-Superior Cervical Ganglion 10 (SCG10) or wheat germ agglutinin labeling (WGA, Cat:#W834, Invitrogen) was performed on 10 μm cryostat sections briefly (5 minutes) brought to room temperature and then re-cooled to -20 degrees C for 30 mins. RGB rightness of the representative images was increased uniformly for presentation purposes.

Mitochondrial occupancy in neuromuscular synaptic junctions was assessed in 10 μm cryostat tibialis muscle sections using anti-COXIV (1:200 in 10 % goat serum) to label mitochondria and anti-acetylcholine receptor with α-Bugarotoxin to label neuronal synapses.

Transmission electron microscopy and toluidine blue staining used standard techniques[15].

Data presentation and statistical analyses

Data are reported as means±SD. Two-group comparisons used Student's t-test; multiple group comparisons used one-way ANOVA, and time-course by treatment group or genotype by

846 treatment group comparisons used two-way ANOVA, with Tukey's post-hoc test for individual
847 statistical comparisons. $P<0.05$ was considered significant.
848 Mouse treatment was randomized according to a random integer table (even or odd) and
849 performed by investigators blind to both genotype and treatment status. Post terminal analysis of
850 tissue and cell phenotypes was performed blindly.
851 *Samples size estimation:* Using two-sample t-test based on the preliminary data where the
852 coefficients of variation (CV) at 50 weeks were 10% and 15% for rotarod latency and
853 CMAP amplitude, respectively, the study was initially designed to have a sample size of 15
854 mice/group, providing 80% power at 1-sided $\alpha=0.05$. Because the therapeutic response for
855 targeted differences was greater than anticipated, the study was completed with a reduced sample
856 size of n=6/group.
857
858

Figures supplement 1-9

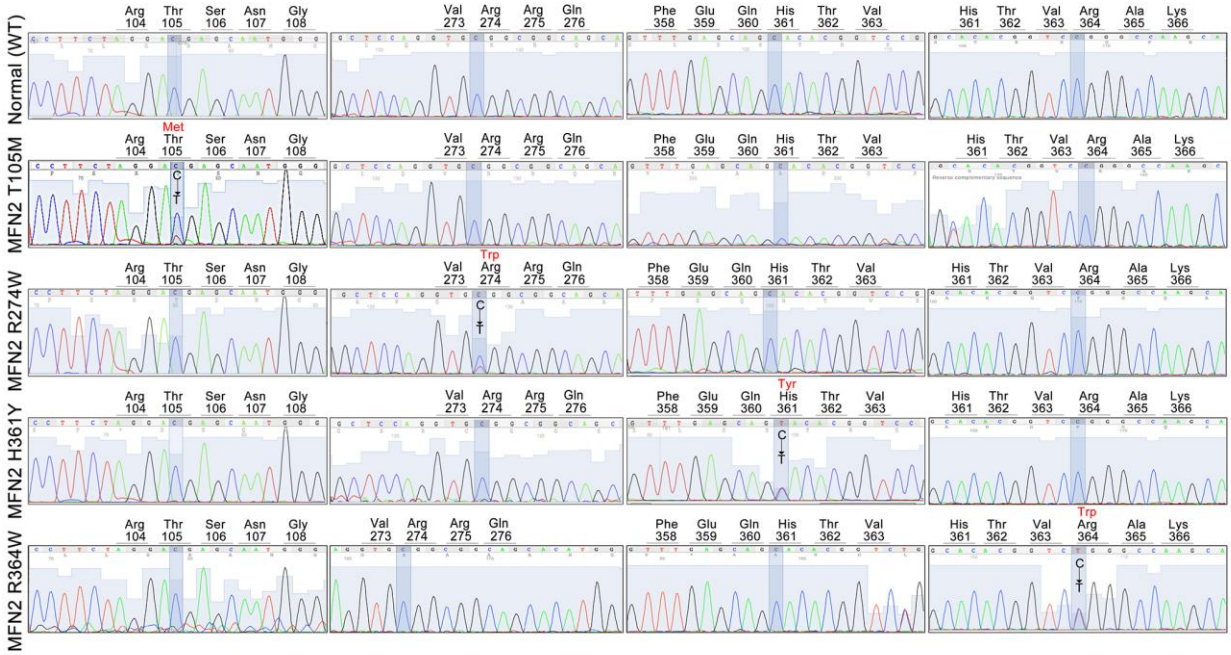

Figure 1 -figure supplement 1. *Genotyping of CMT2A patient cells.* Each cell line underwent Sanger sequencing for all 4 *MFN2* mutation loci. A representative (of 3) normal control lines is shown. Shaded areas show each mutation locus. Encoded amino acids are on top; red amino acid is mutant form.

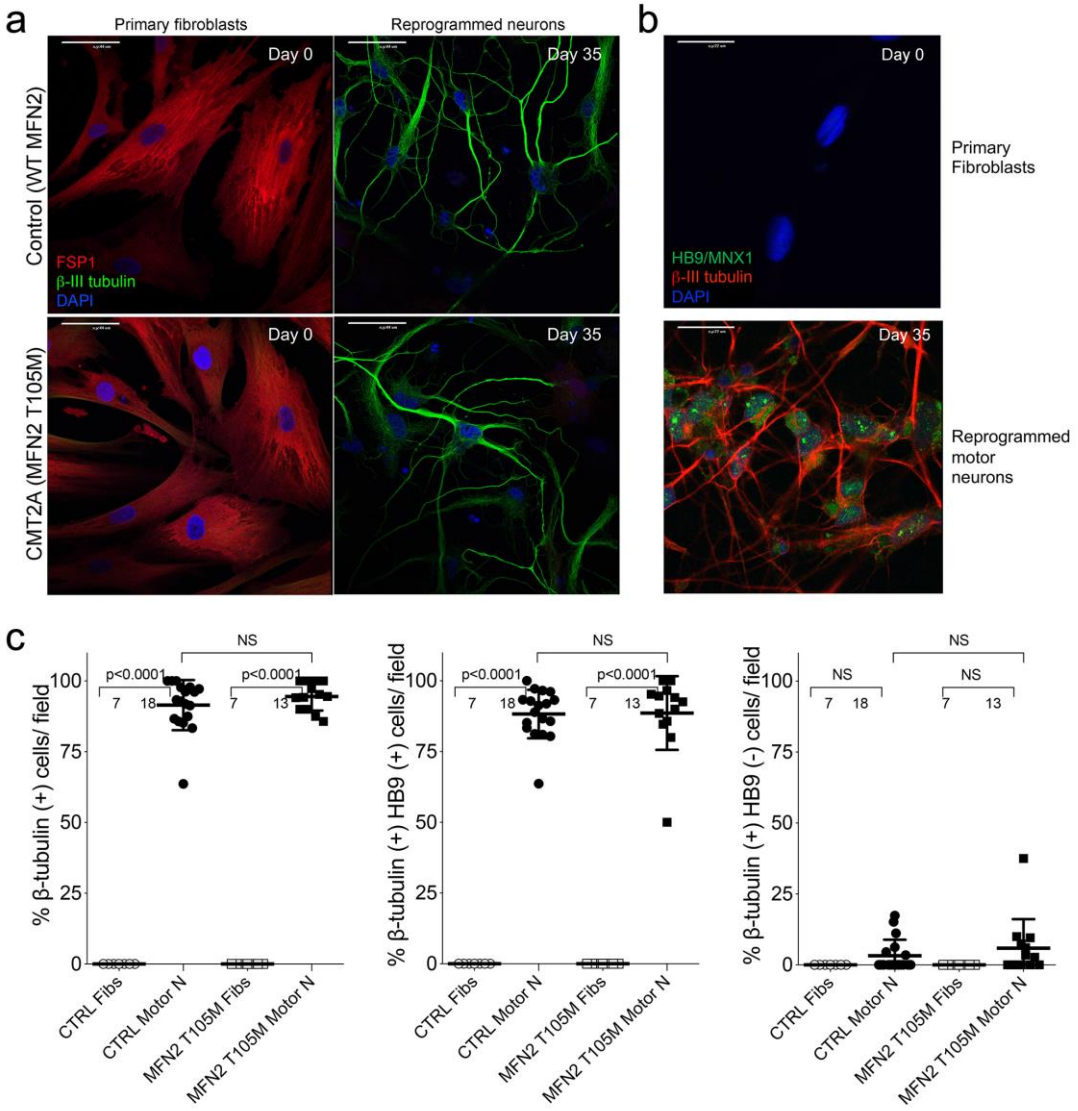

Figure 1 -figure supplement 2. *Direct reprogramming of human skin fibroblasts to neurons.* **a.** Dual immunolabeling of parental fibroblasts (left) and reprogrammed neurons (right) from normal (top) and CMT2A *MFN2* T105M patient (bottom). Red fibroblast specific protein 1(FSP1) labels fibroblasts; green β-III-tubulin labels neurons. **b.** Dual immunolabeling of parental fibroblasts (top) and reprogrammed neurons (bottom) with β-III-tubulin (red) and motor neuron specific HB9/MNX1 (green). **c.** Quantitative data for reprogramming efficiency of control (CTRL) and CMT2A fibroblasts from panels a and b. β-III-tubulin positive cells (left) are neurons; β-III-tubulin positive, HB9/MNX1 positive cells (middle) are motor neurons; β-III-tubulin positive, HB9/MNX1 negative cells are neurons that do not express the motor neuron marker (right). Motor neuron reprogramming efficiency was >90%, and did not differ in CMT2A. P values by ANOVA.

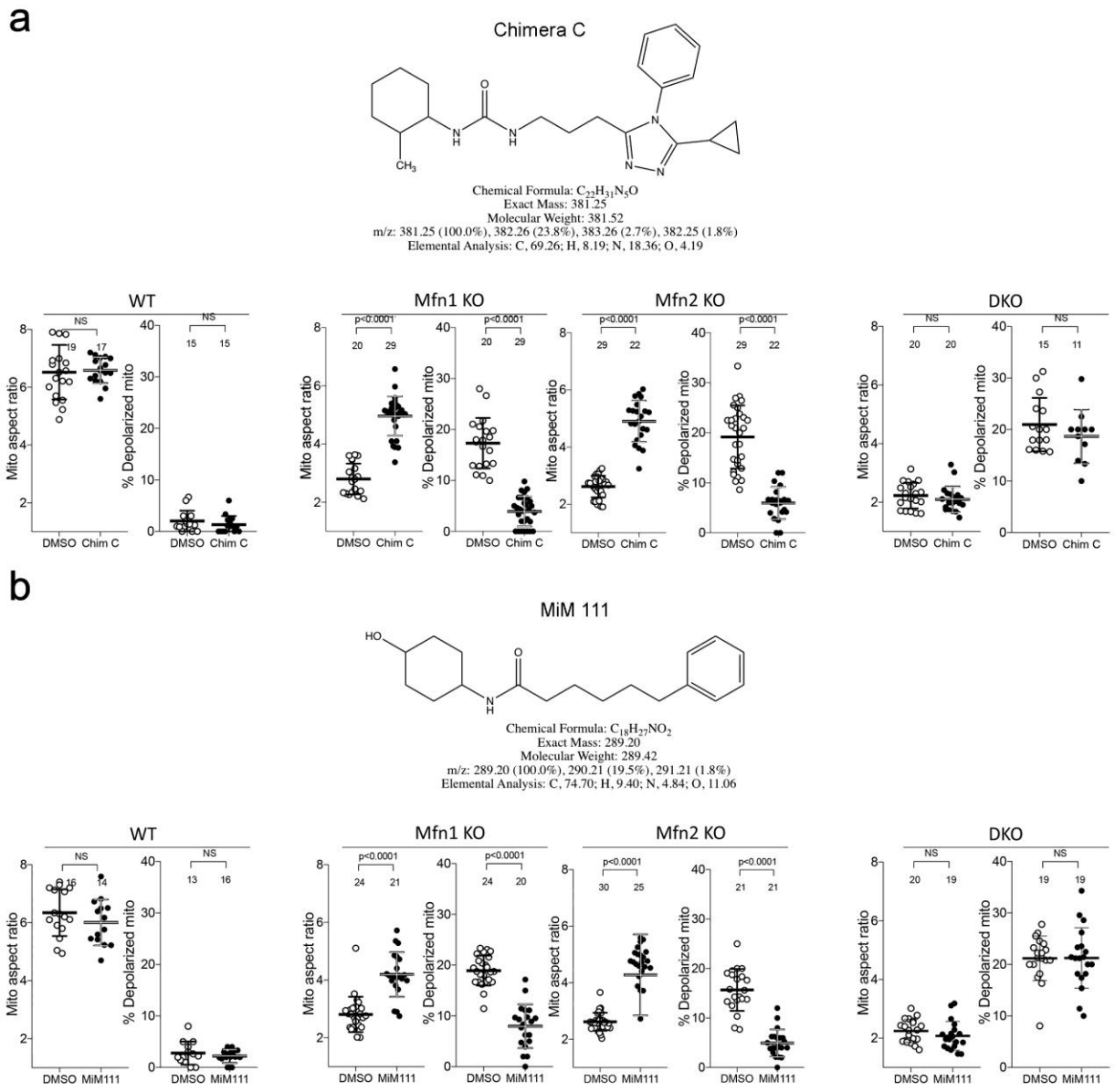

Figure 1 -figure supplement 3. *Chemical characteristics and functional profiling of mitofusin activators used in this study.* **a.** Chimera C is a member of the original chemical class of mitofusin agonists described in reference 23. **b.** MiM111 is the prototype of new chemical class of mitofusin activators having pharmaceutical properties suitable for *in vivo* use, described in reference 25. Quantitative data below each structure show the effects of each compound (100 nM, 48h) on mitochondrial aspect ratio (length/width; a read-out for fusion) and depolarization (indicating respiratory dysfunction) in murine embryonic fibroblasts (MEFs) having different Mfn expression profiles: Wild-type MEFs (left) with both Mfn1 and Mfn2 have normal aspect ratios, low depolarization, and are not affected by mitofusin activation. Mfn1 and Mfn2 KO MEFs (middle) expressing only Mfn2 or Mfn1 respectively have impaired fusion with low aspect ratios, high depolarization, and both of these abnormalities improve with either mitofusin activator. Mfn double knockout MEFs (DKO, right) have no mitofusin targets, so mitochondrial fragmentation and depolarization do not respond to mitofusin activation. P values by t-test.

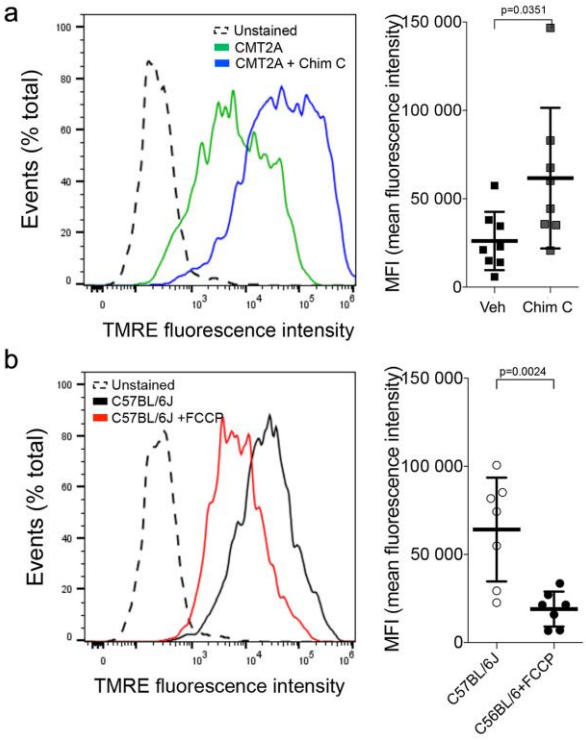

Figure 2 -figure supplement 1. *Flow cytometric profiling of mitochondrial polarization status in mouse dorsal root ganglion (DRG) neurons.* **a.** DRGs from CMT2A MFN2 T105M mice. Left is representative mitochondrial gating by TMRE fluorescence from a single study; green is vehicle; blue is Chimera C (100 nM, 48h). Right graph shows geometric mean fluorescence intensity (MFI) for 8 experiments. TMRE fluorescence is inversely proportional to depolarization; increased fluorescence indicates respiratory fitness. **b.** Control studies as in **a.** using DRGs from normal C57BL/6J mice. FCCP is a depolarizing agent used as a positive control. P values by t-test.

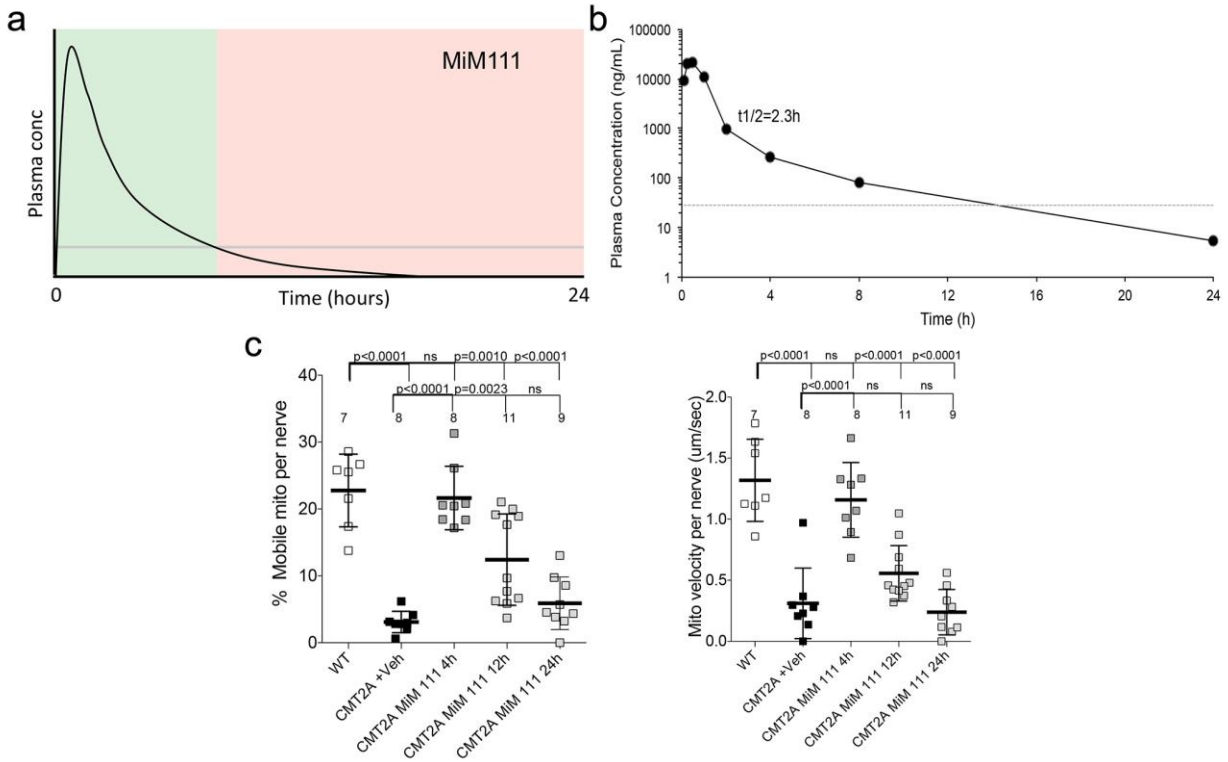

Figure 3 -figure supplement 1. *In vivo pharmacokinetics and target engagement of MiM111 administered intramuscularly.* **a.** Predicted temporal relationship between plasma MiM111 concentration and peripheral nerve mitochondria activation based on published data (reference 25). Green indicates postulated therapeutic levels; pink indicates postulated sub-therapeutic levels. **b.** *In vivo* plasma concentrations of MiM111 after a single dose of 30 mg/kg administered intramuscularly (means of 2 mice). **c.** Time-dependent MiM111 target engagement measured as the increase in proportions (left) and velocity (right) of mobile mitochondria in sciatic nerve axons of CMT2A *MFN2* T105M mice. Each point represents a single neuronal axon, from 2 or 3 mice per time point. WT is normal. P values by ANOVA.

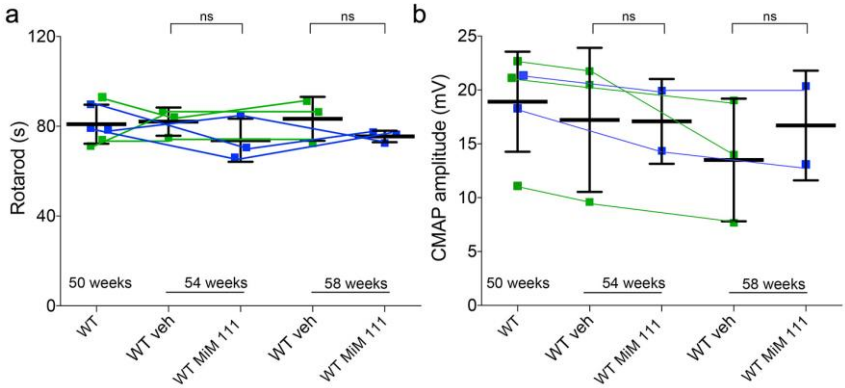

Figure 3 -figure supplement 2. *Effects of MiM111 on neuromuscular function in control mice.* **a.** RotaRod latency. **b.** Neuroelectrophysiologic CMAP amplitude. Each point is a mouse; green is vehicle (n=3), blue is MiM111 30 mg/kg IM once daily (n=3). There were no differences (t-test).

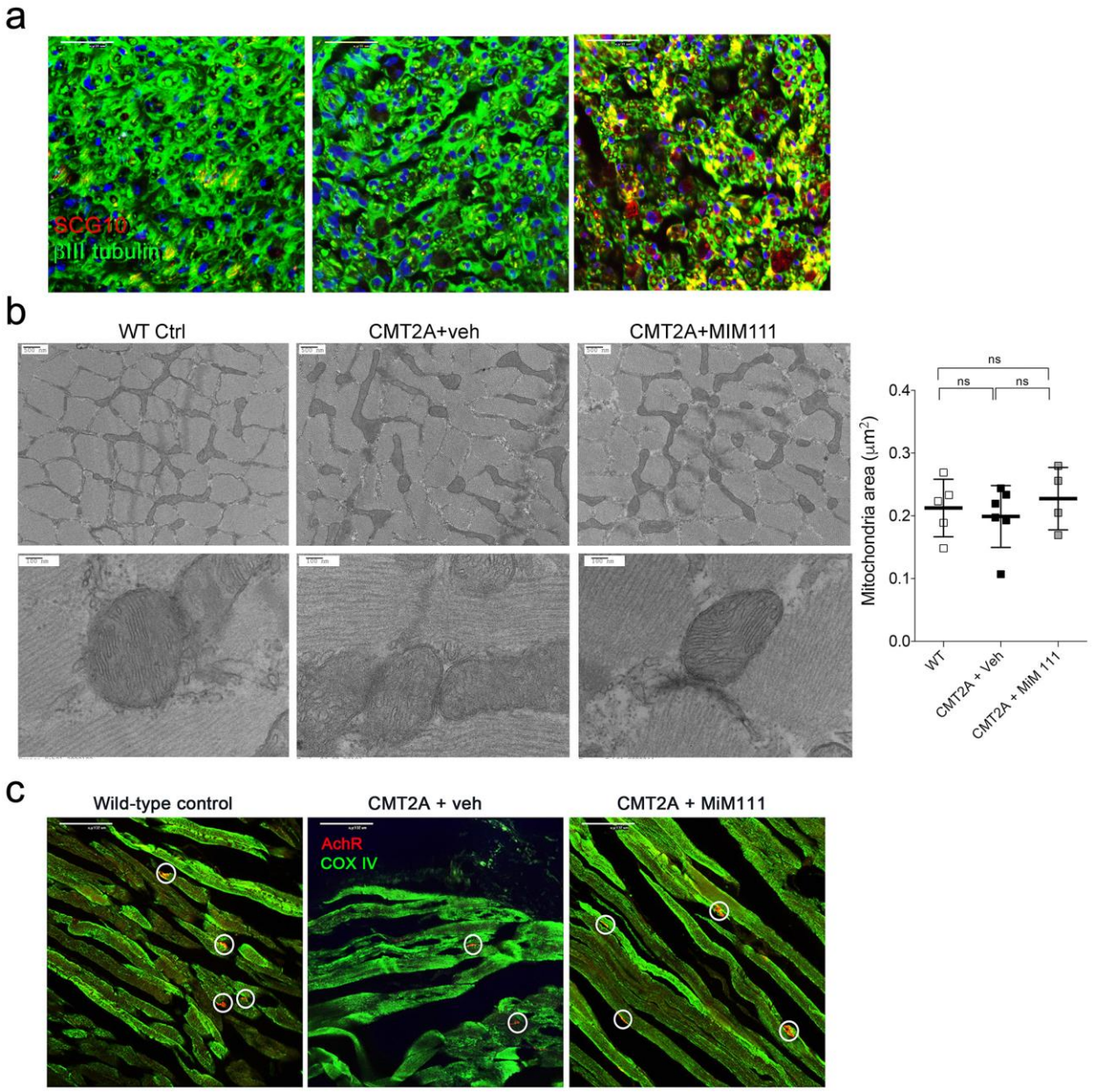

Figure 4 -figure supplement 1. *Effects of MiM111 on neuromuscular integrity in CMT2A MFN2 T105M mice.* **a.** Labeling of regenerating neurons with SCG10 (red). **b.** Mitochondria in tibialis muscles of CMT2A mice are normal. Mitochondrial area is quantified from group data on the right. **c.** Neuromuscular junctional synapses in tibialis muscle of CMT2A MFN2 T105M mice. Acetylcholine receptor (AchR; red) labels terminal neuron synapses (encircled); green is mitochondrial cytochrome C oxidase IV. Quantitative data for panels **a** and **c** are in Figure 4a and 4d, respectively. P values by ANOVA.

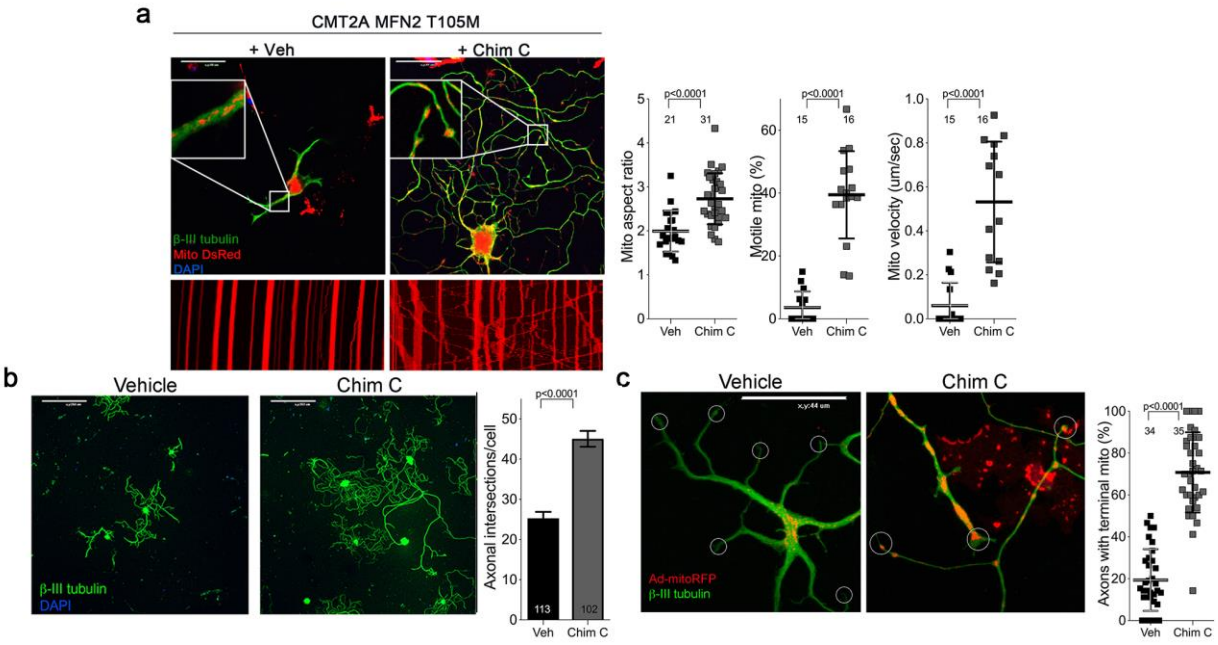

Figure 5 -figure supplement 1. *Mitofusin activation with Chimera C reverses mitochondrial pathology and stimulates growth of CMT2A dorsal root ganglion neurons in vitro.* **a.** CMT2A mouse DRGs cultured for 48h with Chimera C (100 nM) or its vehicle (Me_2SO_4). Exploded insets show mitochondria expressing mitoDS Red; neuronal processes stained for β-III tubulin are green. Kymographs (below) show mitochondrial motility in live cell studies; quantitative group data for aspect ratio and motility are to the right. **b.** Neuronal process length and branching in CMT2A DRG neurons cultured with vehicle or Chimera C. Quantitative group data are to the right. Note greater length and branching of neuronal processes in MiM111-treated neuron. Mitochondria are expressing mitoDS Red. **c.** Proportion of neuronal process termini (encircled) containing mitochondria (red) in vehicle- or Chimera C- treated CMT2A DRGs. P values by t-test.

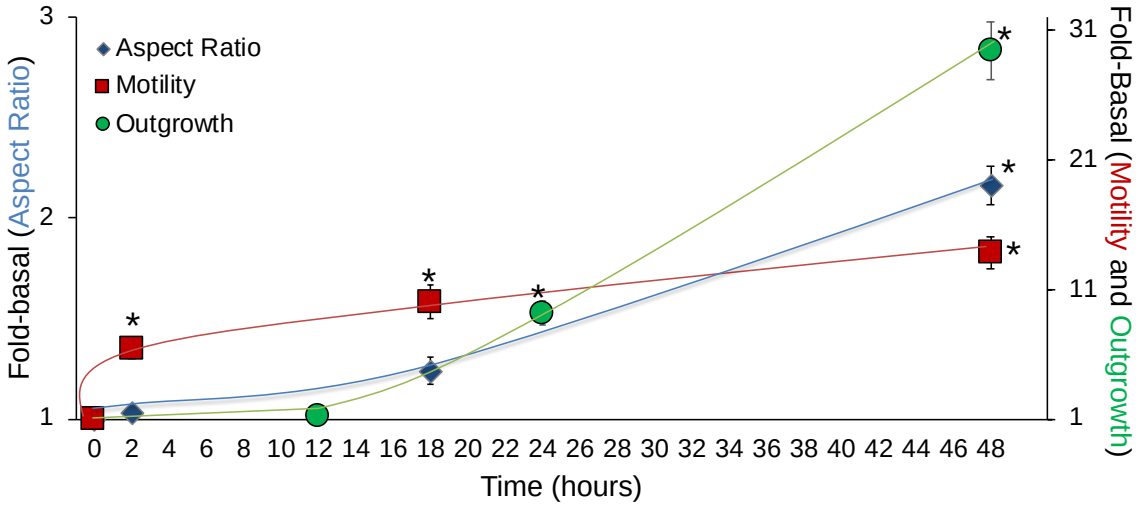

Fugure 5 -figure supplement 2. *Time course studies of DRG mitochondria responses to mitofusin activation after aspiration axotomy.* Studies were performed as in Figure 5. * = P<0.05 vs basal (ANOVA). Three independent studies were performed for each endpoint; each symbol represents the mean value for all three biological replicates, each of which is the average of approximately 3 (mitochondrial motility in different neurons), 20 (outgrowth of different cell neuronal processes), or 300 (aspect ratio of individual mitochondria), technical replicates. The increase in mitochondrial motility (red) was rapid, being half-maximal after 2 hours. The increase in neuron outgrowth (green) was significant after 24h. Increased mitochondrial aspect ratio (blue), reflecting the morphological consequences of enhanced fusion, was only significant after 48 hours.

Key Resources Table				
Reagent type (species) or resource	**Designation**	**Source or reference**	**Identifiers**	**Additional information**
Gene (Mus musculus)	Mfn-2	NCBI Gene	Gene ID: 170731	**MFN2** ENSMUSG00000029020
Gene (Human)	*MFN-2*	NCBI Gene	Gene ID: 9927	MFN2 ENSG00000116688
Genetic reagent (*Mus musculus*)	Rosa-STOP-mMFN Thr105Met (T105M) mice	(C57BL/6 Gt(ROSA) 26 Sortm1 (CAG MFN2*T105M)Dple/)	The Jackson Laboratory: 025322	C57Bl/6
Genetic reagent (Mus musculus)	HB9-Cre mice	(B6.129S1-Mnx1tm4(cre)Tmj/J)	The Jackson Laboratory : 006600	C57Bl/6
Genetic reagent (Mus musculus)	C57BL/6J mice	C57Bl/6	The Jackson Laboratory : 000664	C57Bl/6
Mfn2 null (Mus musculus)	Mfn2 null MEFs	ATCC	CRL-2994	Murine embryonic fibroblasts
Mfn1/Mfn2 null (Mus musculus)	Mfn1 and Mfn2 double knock out MEFs	ATCC	CRL-2993	Murine embryonic fibroblasts
Mfn1 null (Mus musculus)	Mfn1 null MEFs	ATCC	CRL-2992	Murine embryonic fibroblasts
cell line (*Homo-sapiens*)	Dermal fibroblast (MFN2 T105M)	Dr. Robert H. Baloh (Cedars Sinai)		Female
cell line (*Homo-sapiens*)	Dermal fibroblast (MFN2 H361Y)	Dr. Robert H. Baloh (Cedars Sinai)		Male
cell line (Homo-sapiens)	Dermal fibroblast (MFN2 R274W)	Dr. Barbara Zablocka (Mossakowski Med Res Ctr)	**PMID:**28076385	Male
cell line (*Homo-sapiens*)	Dermal fibroblast (MFN2 R364W)	Dr. Michael E. Shy (University of Iowa)		Female
cell line (*Homo-sapiens*)	Dermal fibroblast (Normal)	NINDS	ND34769	Female
cell line (*Homo-sapiens*)	Dermal fibroblast (Normal)	NINDS	ND36320	Female
cell line (*Homo-sapiens*)	Dermal fibroblast (Normal)	NINDS	ND29510	Female

transfected construct (Human Adenovirus Type5 (dE1/E3)	Adenovirus β-galactosidase	Vector Biolabs	Cat#: 1080	
transfected construct (Human Adenovirus Type5 (dE1/E3)	Adenovirus Mito-Ds-Red2	Signagen	Cat#: 12259	
transfected construct (Human Adenovirus Type5 (dE1/E3)	Adenovirus Cre-recombinase	Vector Biolabs	Cat#: 1794	
Recombinant DNA reagent	rtTA-N144 (plasmid)	Addgene	Cat#: 66810	Lentiviral construct to transfect and express the plasmid
Recombinant DNA reagent	pTight-9-124-BclxL (plasmid)	Addgene	Cat#: 60857	Lentiviral construct to transfect and express the plasmid
Recombinant DNA reagent	LHX3-N174 and ISL1-N174 (plasmid)	PMID: 28886366		Lentiviral construct to transfect and express the plasmid
Antibody	anti-Mfn-2 (Mouse monoclonal)	AbCAM	Cat#: ab56889	(1:1000)
Antibody	anti-COX-IV (Rabbit polyclonal)	AbCAM	Cat#: ab16056	(1:1000)
Antibody	anti-Stathmin-2 (Rabbit polyclonal)	Novus Biologicals	Cat#: NBP1-49461	(1:1000)
Antibody	anti-GAPDH (Mouse monoclonal)	AbCAM	Cat#: ab8245	(1:3000)
Antibody	anti-FSP-1 (Rabbit polyclonal)	Novus Biologicals	Cat#: NBP1-49461	(1:400)
Antibody	anti-MNX1 (Mouse monoclonal)	DSHB	Cat#: 81.5C10	(2ug/ml)
Antibody	anti-β-tubulin III (Mouse monoclonal)	Biolegend	Cat#: 801201	(1:200)
Antibody	Alexa-Fluor 488 (Goat anti-mouse)	ThermoFisher	Cat#: A11029	(1:400)
Antibody	Alexa- Fluor 488 (Goat anti-rabbit)	ThermoFishe	Cat#: A11008	(1:400)
Antibody	(Goat anti-rabbit IgG)	ThermoFisher	Cat#: 31460	(1:3000)

Antibody	Alexa- Fluor 594 (Goat anti rabbit)	ThermoFisher	Cat#: A32740	(1:400)
Antibody	(Peroxidase-conjugated anti-mouse IgG)	Cell Signaling	Cat#: 7076S	(1:3000)
Antibody	(α-Bungarotoxin Alexa flour 594)	ThermoFisher	Cat#: B12423	(0.5 µg/ml)
sequence-based reagent	HB9CRE Fw	The Jackson Laboratory	006600	CTAGGCCACAGAATTGAAAGATCT
sequence-based reagent	HB9CRE Rv	The Jackson Laboratory	006600	GTAGGTGGAAATTCTAGCATCATCC
sequence-based reagent	HB9CRE TG Fw	The Jackson Laboratory	006600	GCGGTCTGGCAGTAAAAACTATC
sequence-based reagent	HB9CRE TG Rv	The Jackson Laboratory	006600	GTGAAACAGCATTGCTGTCACTT
sequence-based reagent	Mfn2 T105M M Fw	The Jackson Laboratory	025322	GACCCCGTTACCACAGAAGA
sequence-based reagent	Mfn2 T105M M Rv	The Jackson Laboratory	025322	AACTTTGTCCCAGAGCATGG
sequence-based reagent	Mfn2 T105M Wt Fw	The Jackson Laboratory	025322	AAGGGAGCTGCAGTGGAGTA
sequence-based reagent	Mfn2 T105M Wt Rv	The Jackson Laboratory	025322	CCGAAAATCTGTGGGAAGTC
sequence-based reagent	MFN2 T105M Fw	This paper	PCR primers for cell line mutation validation	TTGCACTGAATAGGGCTTTG
sequence-based reagent	MFN2 T105M Rv	This paper	PCR primers for cell line mutation validation	CATTCACCTCCACAGGGTG
sequence-based reagent	MFN2 R274W Fw	This paper	PCR primers for cell line mutation validation	CGTGGTAGGTGTCTACAAGAAGC
sequence-based reagent	MFN2 R274W Rv	This paper	PCR primers for cell line mutation validation	CTGGTGAGGGCTGATGAAAT
sequence-based reagent	MFN2 H361Y and R364W Fw	This paper	PCR primers for cell line mutation validation	CCTGGCAGTGAAAACCAGAG
sequence-based reagent	MFN2 H361Y and R364W Rv	This paper	PCR primers for cell line mutation validation	AAGGCGTGTCCTAACTGCC

chemical compound, drug	Trans-MiM111	Mitochondria in Motion, Inc	Cpd 13b in PMID: 32506913	
chemical compound, drug	Chimera C	Paraza Pharma	Cpd 2 in PMID: 32506913	
chemical compound, drug	Papain	Sigma	Cat#: P4762	
chemical compound, drug	Laminin	Sigma	Cat#: L2020	
chemical compound, drug	Poly-d-Lysine	Sigma	Cat#: P7886	
chemical compound, drug	Poly-ornithine	Sigma-Aldrich	Cat#: P4957	
chemical compound, drug	Fibronectin	Sigma-Aldrich	Cat#: F4759	
chemical compound, drug	Polybrene	Sigma-Aldrich	Cat#: H9268	
chemical compound, drug	Doxycycline	Sigma-Aldrich	Cat#: D9891	
chemical compound, drug	G418/Geneticin	Invitrogen	Cat# : 10131-035	
chemical compound, drug	Retinoic Acid	Sigma	Cat#: R2625	
chemical compound, drug	BDNF, NT-3, CNTF, GDNF	Peprotech	Cat#: 450-02, Cat#: 450-03, Cat#: 450-13, Cat#: 450-10	
chemical compound, drug	Dibutyryl cAMP	Sigma	Cat#: D0627	
chemical compound, drug	Valproic acid	Sigma	Cat#: 676380	
chemical compound, drug	Puromycin	Invitrogen	Cat#: A11138-03	
chemical compound, drug	Collagenase	Worthington Biochemical	Cat#: 41J12861	
chemical compound, drug	(2-Hydroxypropyl)-β-cyclodextrin	Sigma	Cat#: 332607	
chemical compound, drug	Carbonyl cyanide-*p*-trifluoromethoxyphenyl hydrazone	Sigma	Cat#: C2759	
chemical compound, drug	B27 Supplement	Gibco	Cat#: 17504-044	
chemical compound, drug	Insulin-Transferrin-Sodium Selenite	Sigma	Cat#: 1884	
chemical compound, drug	Glucose	Sigma	Cat#: G5767	

chemical compound, drug	L-Glutamine	Gibco	Cat#: 25030-149	
chemical compound, drug	Goat serum	Jackson Immunoresearch	Cat#: 005-000121	
chemical compound, drug	Glutaraldehyde	Electron Microscopy Science	Cat#: 16216	
chemical compound, drug	MitoTracker Green	Thermo Fisher	Cat#: M7514	
chemical compound, drug	Calcein AM	Thermo Fisher	Cat#: C3100MP	
chemical compound, drug	Hoechst	Thermo Fisher	Cat#: H3570	
chemical compound, drug	MitoTracker Orange	Thermo Fisher	Cat#: M7510	
chemical compound, drug	Tetramethylrhodamine ethyl ester	Thermo Fisher	Cat#: T-669	
software, algorithm	ImageJ	C. A. Schneider	https://imagej.net/Sholl_Analysis	
software, algorithm	Viasys Healthcare Nicolet Biomedical instrument with Viking Quest version 11.2 software	Middleton	Cat#: OL060954	
software, algorithm	Gallios instrument with FlowJo 10 software	Beckman Coulter	N/A	
other	RotaRod	Ugo Basile	Cat#: 47650	
other	XonaChips	Xona Microfluidics	Cat#: XC450	